EXPLORING GLOBAL AND MICRO-ENVIRONMENT CONDITIONS FOR AFFECTING ENZYME ACTIVITIES AND FUNCTIONAL TRANSITIONS

By

JOHN COLLINS

A thesis submitted to the

Graduate School – Camden

Rutgers, The State University of New Jersey

In partial fulfillment of the requirements

For the degree of Master of Science

Graduate Program in Chemistry

Written under the direction of

Jinglin Fu

And approved by

_____

Jinglin Fu, Ph.D.

_____

David Salas-de la Cruz, Ph.D.

_____

Hao Zhu, Ph.D.

Camden, New Jersey

October 2017

THESIS ABSTRACT

Exploring global and micro-environment conditions for affecting enzyme activities and functional transitions

By JOHN COLLINS

Thesis Director:

Jinglin Fu, Ph.D.

The metabolism of living systems utilize many biosynthetic pathways in order to maintain homeostasis. These metabolic pathways involve multi-step chemical reactions to synthesize molecules and convert energy that are vital to life. These reactions, however, are too slow to support life. Nature has evolved enzymes, which are macromolecular catalysts, to speed up and catalyze these metabolic reactions. Enzymes are very sensitive to their surrounding environment, which can have profound effects on the enzymes function. In this thesis, the effects of different environments on the function of enzymes are explored. First, the effects of an anaerobic environment are shown to add a new catalytic function to an enzyme, allowing an FMN-bound diaphorase to act as a transhydrogenase, transferring a hydride between two critically important metabolic cofactors, NAD and NADP. Second, the effects of the storage conditions of the enzyme diaphorase are explored, and how its catalytic function changes from a dehydrogenase to that of an oxidase due to do partial unfolding of the enzyme during prolonged storage. Third, a DNA-crowded enzyme complex was developed to increase the local molecular crowding for affecting enzyme functions. The DNA-crowded enzyme nanoparticles are

made by directly growing double-strand DNA on the enzymes surface via the hybridization chain reaction. The experimental results show that enzymes become more active and stable under a local DNA-crowded nano-environment.

TABLE OF CONTENTS

Page

LIST OF TABLES

LIST OF FIGURES

Chapter 1

Introduction and Background

Abstract

In this chapter, a general overview of enzymes and their functions will be discussed, including the mechanisms how enzymes work, the surrounding environment affecting enzyme activities, and the industrial/medical applications of enzymes. This chapter also discusses DNA nanotechnology, and how to engineer enzyme/DNA hybrid nanostructures.

1.1. Overview of Enzymes

The metabolism of living systems utilize many biosynthetic pathways in order to maintain homeostasis.[1] These metabolic reactions are often complex, and tend to involve multi-step reactions.[2] Many of these reactions, however, have slow reaction kinetics, and take place on time scales that are too long for life to even exist.[3] To overcome this feat, nature created enzymes. Enzymes are protein based macromolecules that function as catalysts. As seen in **Figure 1**, they work by lowering the activation energy required for the reaction. This, in turn, speeds up the reaction kinetics, with rate enhancements on the order of 10^6-10^{17}.[4] While enzymes may be able to drastically increase the rate of a reaction, they cannot catalyze reactions with unfavorable changes in free energy. Enzymes are very specific in the reactions they catalyze, typically only catalyzing one type of reaction, and only with specific substrate molecules. The way in which enzymes

catalyze reactions can be seen in **Figure 2**. Enzymes work by first binding to the substrate(s) at the active site, and lowering the activation energy of the reaction. This lowering of the activation energy is achieved due to the microenvironment inside the active site that favors binding of the transition state, which stabilizes it. By stabilizing the transition state, the enzyme decreases the activation energy required for the reaction, greatly enhancing the rate for the formation of product.

Figure 1. Gibbs free energy of (a) an uncatalyzed reaction (red curve) and (b) enzyme-catalyzed reaction (blue curve).[5]

Figure 2. Cartoon representation of enzymatic catalysis.[6] In the first step, the substrate binds to the enzymes active site. Then, in the second step, the enzyme holds the substrate in place through weak interactions, such as hydrogen bonding and electrostatics. During the third step, the activation energy of the reaction is lowered. During the fourth step of catalysis, the substrate molecule(s) is converted to product(s). The product molecule(s) is then released in the fifth step. Then finally (step 6), the enzyme is unbound, and able to bind to new substrate molecule(s).

Most enzymes are globular proteins, which are roughly spherical in shape. Although most enzymes have roughly the same three dimensional shape, they can vary differently in size, and in the number of polypeptide chains that make up the enzyme. For example, the enzyme ribonuclease A (from bovine pancreas) is a 124 amino acid peptide with a molecular weight of 12,400 g/mol.[7] This is small in comparison to the enzyme glutamine synthetase (from E. coli), which contains 5,628 amino acids residues formed

from 12 distinct polypeptides.[7] While enzymes can vary greatly in terms of size, they typically only have 3-4 amino acids in the active site that are responsible for catalysis.[7]

Enzymes are very sensitive to their environment. Factors such as temperature, pH, ionic strength, and the presence of organic solvents can have a profound impact on the ability of an enzyme to catalyze reactions.[8] Elevated temperatures add more energy to the system. This allows chemical reactions to take place at faster rates, and allows molecules to have an easier time undergoing conformational transitions. Since the activity of an enzyme is related to its three dimensional structure, elevated temperatures can cause enzymes to unfold, decreasing their activity.[8b] Changes in pH can change the protonation state of an enzyme. This can have a significant effect on the activity of an enzyme if a specific protonation state is needed for key amino acids involved in catalysis.[8] Likewise, ionic strength is crucial to catalysis. Salts can be essential for catalysis by forming salt bridges in the active site, or by stabilizing the active conformation of the enzyme.[7] Low ionic strengths tend to destabilize enzymes, while high ionic strengths can cause unwanted aggregation.[7, 8b] Some enzyme substrates have poor water solubility, and thus the use of organic solvents cannot be avoided in some instances when trying to measure the kinetic parameters of certain substrates.[8b] Organic solvents can also cause enzymes to denature, by preferentially solvating the hydrophobic core of enzymes.[7]

One of the most common models for explaining the enzyme kinetics was developed by Leonor Michaelis and Maud Menten in 1913.[7] They describe an enzyme catalyzed reaction (involving a single substrate) as a two-step process. First, the substrate binds to the enzyme to from the enzyme-substrate complex. This step is a fast, reversible process, where the enzyme-substrate complex can either continue on to the next step of

the reaction to form product, or dissociate back to substrate and enzyme. The second step of the reaction is the rate-limiting step, in which the enzyme-substrate complex breaks down, forming both the free enzyme and the reaction product. Because of this two-step process, the reaction rate is dependent on the concentration of the enzyme-substrate complex. When the substrate concentration is low, the concentration of the enzyme-substrate complex is also correspondingly low. As the concentration of the substrate is increased, the concentration of enzyme-substrate complexes increases, giving rise to increased reaction rates. This effect holds up to a certain point, in which increasing the concentration of substrate does nothing to increase the reaction rate. This maximum reaction rate, V_{max}, is achieved when the concentration of the enzyme-substrate complex far exceeds that of the free enzyme. In this case, the enzyme is said to be saturated with its substrate.

The relationship between the concentration of substrate, and the rate of an enzyme catalyzed reaction can be expressed quantitatively using the Michaelis-Menten equation (**Figure 3**).

Figure 3. Michaelis-Menten model of enzyme kinetics. Plot of enzyme velocity as a function of substrate concentration. The Michaelis-Menten equation is shown in the upper left hand corner of the graph.[8b]

Where V_o is the reaction rate measured during the initial time period of the reaction, [S] is the concentration of substrate, V_{max} is the maximum rate of reaction, and K_m, which is known as the Michaelis constant. The Michaelis constant is equal to the substrate concentration needed for the reaction rate to equal one half the maximum rate.

The activity of enzymes can also be modulated in the presence of other molecules (typically small molecules).[7] Many enzymes are allosterically regulated, where binding of a molecule can either inhibit or activate the enzyme. For example, some enzymes are

inhibited by the substrate on which they act on at high substrate concentrations. In addition to substrate inhibition, most modern medicines are small molecule drugs that work by binding to an enzyme and inhibiting its activity through one of four mechanisms. These mechanisms of inhibition are competitive, non-competitive, uncompetitive, and mixed. In competitive inhibition (**Figure 4B**), the inhibitor molecule binds directly to the active site of the enzyme, preventing substrate molecules from binding. Competitive inhibitors tends to have structures that mimic the substrate, but bind with greater affinity to the active site. This causes an apparent increase in K_m, leaving V_{max} unchanged. Non-competitive inhibitors (**Figure 4C**) work by binding to an enzyme at a site other than the active site. This causes a decrease in V_{max}, leaving K_m unchanged. An uncompetitive inhibitor (**Figure 4D**) works by binding directly to the enzyme-substrate complex, preventing the enzyme from converting substrate to product. Experimentally, this causes a decrease in both V_{max} and K_m. Mixed inhibition is difficult to describe in that it effects both binding of substrate to the enzyme, and the maximum rate of the reaction. Both K_m and V_{max} are altered, however, the ratio of K_m to V_{max} is not constant compared to the other forms of inhibition.

Figure 4. Kinetics of enzyme inhibition represented using Lineweaver-Burke plots. (A) Uninhibited enzyme catalyzed reaction. (B) Enzyme catalyzed reaction inhibited by a competitive inhibitor. (C) Enzyme catalyzed reaction inhibited by a noncompetitive inhibitor. (D) Enzyme catalyzed reaction inhibited by an uncompetitive inhibitor.[9]

Enzymes find use in a wide variety of industrial applications, such as in the production of fine chemicals,[10] pharmaceuticals,[11] cosmetics,[12] food,[13] textiles,[14] and paper.[15] This is due to their high catalytic efficiency and specificity, as well as providing a green alternative to traditional chemical catalysts. The only drawback to using enzymes in industrial applications, however, is their poor stability under elevated temperatures, and in the presence of organic solvents.[16] Protein engineering methods, such as directed evolution and structure-based rational design, have allowed scientists to fine tune enzymes in order to increase their activity and stability, as well as broaden the range of

substrates for which the enzyme can act on. In addition to protein engineering methods, screening for various activities from extremophiles has allowed scientists to discover novel enzymes which are active under extremes of temperature, pH, and ionic strength.[16]

1.2. Enzymes in the Cellular Environment

Since the inception of enzymology, biochemists would study and characterize enzymes by measuring their kinetics in a dilute aqueous solution.[17] To this day, enzymes are still characterized in this way. In these experiments, the concentration of enzyme is typically on the order of 10^{-9} M, with substrate concentrations typically in the range of 10^{-6} to 10^{-3} M.[8b] While these *in vitro* conditions allow us to simply measure the kinetic properties of an enzyme, they do not fully represent how the enzyme functions *in vivo*. This is due to the fact that the interior of a cell is a highly crowded environment. The inside of a cell is packed with proteins, polysaccharides, and nucleic acids. The concentration of these biological macromolecules inside the cell can be as high as up to 400 mg/mL,[18] corresponding to a volume occupancy of 40%.[19] At such a high volume occupancy, the amount of free water is considerably low, with a high population of water molecules bound to, or solvating other molecules.[20] While the total concentration of bio-macromolecules is high, the concentration of any individual bio-macromolecule is low, which is why the term ‘crowded’ is used.[21]

Due to the extent of molecular crowding inside of a cell, the volume occupied by solutes is unavailable to other solutes, simply because no two molecules can exist in the same space at the same time. This can have significant effects on reactions or processes taking place inside the cell that depend on the available volume. These are known as

excluded volume effects.[22] Thermodynamically, this is described as an increase in the activity of the solute. The randomness of a particles distribution decreases as the available volume decreases (**Figure 5)**. This leads to a decrease in the entropy of the solution, giving rise to the increase of the thermodynamic activity of the solute.[22] This makes sense given that proteins are not structurally rigid, but are capable of intramolecular movements and undergoing conformational transitions. By reducing the space available, you reduce the enzymes ability to move in this way. Therefore, the behavior of an enzyme inside of a cell is expected to be different than in a dilute solution.

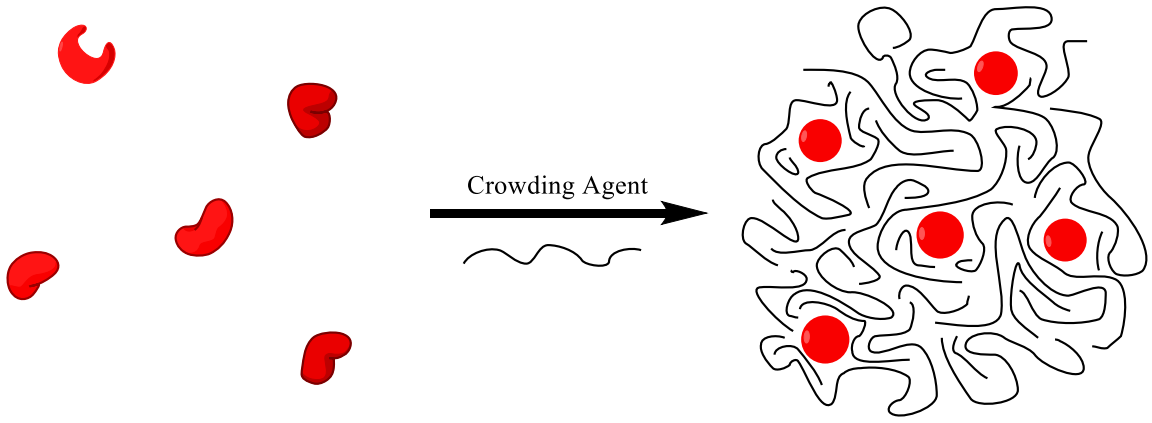

Figure 5. Effects of molecular crowding on the structural dynamics of enzymes. Under molecular crowding conditions, the randomness of an enzymes structure decreases as the available volume decreases.

Due to the excluded volume caused by molecular crowding, the equilibria that govern specific biological processes can be significantly affected. These processes include protein folding, enzyme activity, protein-protein interactions, as well as aggregation. For example, the activity of Glucose-6-phosphate Dehydrogenase (G6PDH) is significantly enhanced under molecular crowding conditions. G6PDH can exist as a monomer, dimer, or tetramer. The dimeric form, however, is the only active form of the enzyme. It was shown that under molecular crowding conditions, the activity of G6PDH was enhanced to due favored formation of the dimeric form of the enzyme, even under destabilizing conditions.[23] Not all changes in equilibrium caused by molecular crowding lead to desirable changes in activity or stability. For example, the aggregation of denatured β-lactoglobulin into amyloid fibrils is accelerated under molecular crowding conditions.[24] Under normal assay conditions, it takes 20 days for the Guanidinium Hydrochloride (GdmHCl) mediated unfolding and aggregation into amyloid fibrils. Under crowded conditions using dextran and PEG, however, it was found that the formation of amyloid fibrils can be greatly accelerated.

There are two main approaches biochemists use to study the effects of molecular crowding on protein structure and function. The first involves adding a high concentration of a "molecular crowding agent" to a solution containing the protein of interest. At high concentrations, the molecular crowding agent is able to exclude a large portion of the available volume in solution, mimicking the crowded cellular environment. Typically, an inert polymer is used as the molecular crowding agent, such as polyethylene glycol (PEG), ficoll, dextran, or proteins such bovine serum albumin (BSA).[17] The other approach involves the encapsulation of the protein of interest,

confining it inside of a tight space to mimic the cellular environment. To accomplish this scientists tend to encapsulate enzymes inside of liposomes,[25] polymersomes,[26] and sol-gels.[27]

One explanation for significant changes in the biological activity of enzymes under molecular crowding conditions, compared to enzymes in dilute solutions, is due to a change in the way in which water behaves. A recent study by King et. al. used two-dimensional infrared spectroscopy (2D-IR) to study the picosecond protein and hydration dynamics of lysozyme under various crowding conditions.[28] They observed a sharp transition in the protein and hydration dynamics when the percent volume of water reaches a critical value. They attribute this sharp transition to an independent to collective hydration of lysozyme, in which the water molecules involved in hydrating the dissolved enzyme fuse together. This leads to a slowing of the hydration dynamics of water molecules by up to an order of magnitude relative to that of water in the bulk solution. Simulations suggest that when molecules of lysozyme are within 3-4 nm of each other, that the enzymes become collectively hydrated.

1.3. Assembly of Enzymes on DNA Nanostructures

DNA nanotechnology is a bottom-up approach involving the self-assembly of individual strands of nucleic acids to form structures at the nanoscale, with defined structural properties. The first ever DNA nanostructure was reported by Nadrian Seeman in 1982, in his pioneering work “Nucleic acid junctions and lattices”.[29] In this work, Seeman demonstrated the potential utility of DNA as a nanoscale building material when

he was able to assemble a highly ordered lattice structure using only nucleic acid hybridization. Since then, many different DNA nanostructures have been created.[30]

Currently, there are two popular methods for creating DNA nanostructures: 1) DNA origami,[31] and 2) DNA tiles/bricks.[32] As seen in **Figure 6**, DNA origami involves the programmed folding of a large, circular DNA "scaffold strand" (typically M13 bacteriophage DNA) into a user defined shape. The DNA origami structure is held together through the use of "staple strands", which are short oligonucleotides that bind to different portions of the scaffold strand and hold the nanostructure together. In DNA tiles (**Figure 7**), short single stranded tile strands are used to form a large molecular canvas of DNA, from which various DNA nanostructures can be realized. The tile strands are 42 base pair long oligonucleotides, each of which contains four binding domains. The binding domains allow the tile strands to hybridize with each other, in a matter similar to stacked 2x1 Lego pieces, where binding domains 1 and 4 of one tile strand, bind to domains 3 and 2 of two other tile strands respectively. This allows a molecular canvas of DNA to be formed. By simply not including all strand species of the canvas from the strand mixture, various DNA nanostructures are formed. This concept can be further applied to three dimensional nanostructures, where the term DNA bricks is used in place of DNA tiles to represent the construction of a three-dimensional structure.

Figure 6. Schematic representation of the formation of DNA origami structures.

Figure 7. Schematic representation of the formation of DNA brick structures.[32a] (A) Secondary structural representation of a DNA brick. (B) Schematic representation of the hybridization of two DNA bricks. (C) A fully formed DNA brick canvas.

Due to the well-defined structural features of DNA, DNA nanotechnology offers a means to site-specifically incorporate functional elements onto a DNA scaffold with nanoscale precision. Materials such as inorganic nanoparticles,[33] enzymes,[34] and aptamers[35] have all been incorporated into DNA nanostructures to give them various functions. For example, Fu et. al used a DNA origami tile to position two enzymes involved in an enzymatic cascade in close proximity (**Figure 8A**).[2] They showed the activity of the cascade was enhanced in a distance dependent manner, with the highest

activity being realized when the enzymes were positioned ten nanometers apart. By positioning the enzymes together in close proximity, the activity was enhanced due to substrate channeling between the two enzymes. Work done by Liu et. al (**Figure 8B**) used a DNA tweezer design to create an enzyme-cofactor system that can be turned on and off by the use of a DNA fuel strand.[36] When the tweezer is in the open position, G6PDH and its cofactor NAD+ are positioned six nanometers apart. This is far enough away to keep the rate of reaction low. Upon the addition of a fuel strand, the tweezer is able to close, and the activity of the enzyme-cofactor system is boosted almost six-fold, due to the close proximity of G6PDH to NAD+. In another paper by Fu et. al. (**Figure 8C**), they demonstrated that enhanced catalysis can be realized through the positioning of a NAD modified artificial swinging arm between two enzymes involved in a cascade reaction which utilized this cofactor.[37] Enhanced catalysis was realized in this system because of the locally high effective concentration of the cofactor, due to it being unable to diffuse into the bulk solution. The use of the swinging arm was also able to prevent unwanted side reactions, which was demonstrated through a competition based assay with a competing enzyme present in the bulk solution.

Figure 8. Functionalization of DNA nanostructures. (A) Assembly of the Glucose Oxidase (GOx) and Horseradish Peroxidase (HRP) enzyme cascade, with controllable distances, on a DNA origami scaffold.[2] (B) A DNA tweezer functionalized with a G6PDH-NAD enzyme-cofactor pair, that can be turned on or off with the addition of a fuel/set DNA strand.[36] (C) An enzyme cascade anchored on a DNA scaffold, with a NAD artificial swinging arm to facilitate substrate channeling.[37]

More interestingly, DNA nanostructures can also affect enzyme activity in an enzyme-DNA nanostructure. Several published studies have demonstrated that enzymes incorporated into DNA nanostructures have enhanced catalytic activity and stability compared to free enzymes in solution. For example, a study in 2012 by Rudiuk et. al. showed that an enzyme attached to long double stranded DNA showed an almost 2-fold enhancement in catalytic efficiency compared to the free enzyme.[38] In another work, Timm C. et. al. demonstrated that enzymes attached to DNA nanostructures showed resistance to degradation during purification compared to free enzyme controls.[39] A more recent paper by Zhao et. al. demonstrated, with multiple enzymes, that enzymes encapsulated inside of a DNA cage had greatly enhanced activity, with up to 5-fold enhancements in catalytic efficiency.[40] As seen in **Figure 9**, they noticed that as the amount of DNA surrounding the enzyme was increased, a larger enhancement in activity was observed. The observed enhancement in enzyme activity and stability has been attributed to the large negative charge present in DNA nanostructures. It is possible that DNA can function as a molecular chaperone, keeping the enzymes in their active conformations. A study by Gray et. al. recently showed the poly inorganic phosphate (which carries a large negative charge, like DNA) can act as a molecular chaperone. Gray et. al. demonstrated that polyphosphate could prevent the inactivation and aggregation of proteins under various stress conditions, such as temperature, pH, and oxidation.[41]

Figure 9. Enzymes encapsulated inside of a DNA nanocage show enhanced catalytic activity. (A) Cartoon representation of the design and assembly of the DNA nanocage. (B & C) TEM images demonstrating the encapsulation of one (b) or two (c) enzymes inside of the DNA nanocage. (D) Bar graph demonstrating the enhancement in the rate constant (kcat), and change in Km, as the density of DNA around the enzyme increases.

1.4. Conclusion

In this thesis, the impact of the surrounding environment on an enzymes activity will be discussed. In chapter 2, I will discuss the effects of removing dissolved oxygen on the activity of a NADH dehydrogenase known as diaphorase, and how it gains a new transhydrogenase activity under such conditions. In chapter 3, I will discuss the effects of the prolonged storage of diaphorase, and how partial unfolding of the protein causes its function to change from that of a dehydrogenase, to that of an oxidase. Finally, in chapter 4, I will discuss our method for creating DNA-crowded enzyme nanoparticles, and how the local molecular crowding effect caused by the DNA creates a micro-environment that can enhance the activity and stability of several enzymes.

Chapter 2

A Hidden Transhydrogen Activity of a FMN-Bound Diaphorase under Anaerobic Conditions

Abstract

The redox cofactors NADH and NADPH participate in many cellular metabolic pathways for facilitating the electron transfer from one molecule to another in redox reactions. Transhydrogenases play an important role in linking catabolism and anabolism, regulating the ratio of NADH/NADPH in cells. Cytoplasmic transhydrogenases could be useful to engineer synthetic biochemical pathways for the production of high-value chemicals and biofuels. A transhydrogenase activity was discovered for a FMN-bound diaphorase (DI) from *Geobacillus stearothermophilus* under anaerobic conditions. The DI-catalyzed hydride exchange was monitored and characterized between a NAD(P)H and a thio-modified NAD^+ analogue. This new function of DI was demonstrated to transfer a hydride from NADPH to NAD^+ that was consumed by NAD-specific lactate dehydrogenase and malic dehydrogenase. In the future, it may be possible to incorporate this FMN-DI into synthetic enzymatic pathways for balancing NADH generation and NADPH consumption for anaerobic production of biofuels and biochemicals.

2.1. Introduction

Cellular metabolism uses many cofactors for facilitating the electron transfer from one molecule to another in redox reactions. Although chemically similar, nicotinamide adenine dinucleotide (NAD^+) and nicotinamide adenine dinucleotide phosphate ($NADP^+$) serve distinct biochemical functions in metabolism. NADH mainly participates in catabolism and provides reducing power for oxidative phosphorylation (electron-transport chains in mitochondria), generating ATP from ADP.[42] Conversely, NADPH exclusively drives the anabolic synthesis of important biomolecules, such as lipids, amino acids and sugars,[43] as well as the reduction of glutathione.[44] Transhydrogenases play an important role in linking catabolism and anabolism, regulating the ratio of NADH/NADPH in cells.[45] Proton-translocating transhydrogenase's are also important in bioenergetics, where the hydride transfer from NADH to $NADP^+$ is powered by an electrochemical proton gradient in mitochondria.[43b, 46] Though important, many of natural transhydrogenases are membrane-bound proteins with poor solubility and low stability in aqueous solution.[45] Several efforts have been reported to express and purify soluble transhydrogenases with improved stability.[47] The discovery of novel cytoplasmic transhydrogenases could find utility in a number of synthetic biology applications, such as metabolic engineering and the production of high-value chemicals and biofuels.

Diaphorase (DI), a soluble NAD(P)H dehydrogenase (EC 1.6.99.1 or EC 1.6.99.3), has been found to catalyze the electron transfer from a NAD(P)H to a variety of electron acceptors, such as methylene blue,[48] resazurin,[49] vitamin K_3,[50] azo dyes[51] and AQDS.[52] As shown in **Figure 10A**, a flavin mononucleoide (FMN) is bound to a protein monomer, which serves as a redox center for catalyzing the electron transfer.[53] Oxidized

FMN-DI has a strong absorbance at 452 nm (**Figure 10B**), and can be reduced to $FMNH_2$-DI by accepting two electrons from a NAD(P)H. The reduced $FMNH_2$-DI can then donate a pair of electrons to an electron acceptor. Due to its versatile functions as a NAD(P)H dehydrogenase, FMN-DI has been widely applied to the redox sensing of cofactors and enzymatic fuel cells.[50, 54] FMN-DI also shows NAD(P)H oxidase (EC 1.6.3.1) activity under aerobic conditions,[55] where molecular oxygen is reduced to H_2O_2 by accepting electrons from NAD(P)H. Here we report for the first time that a FMN-DI, under anaerobic conditions (i.e., the removal of dissolved oxygen in an aqueous solution), can function as a transhydrogenase that catalyzes the exchange of a hydride between NADH and NADPH.

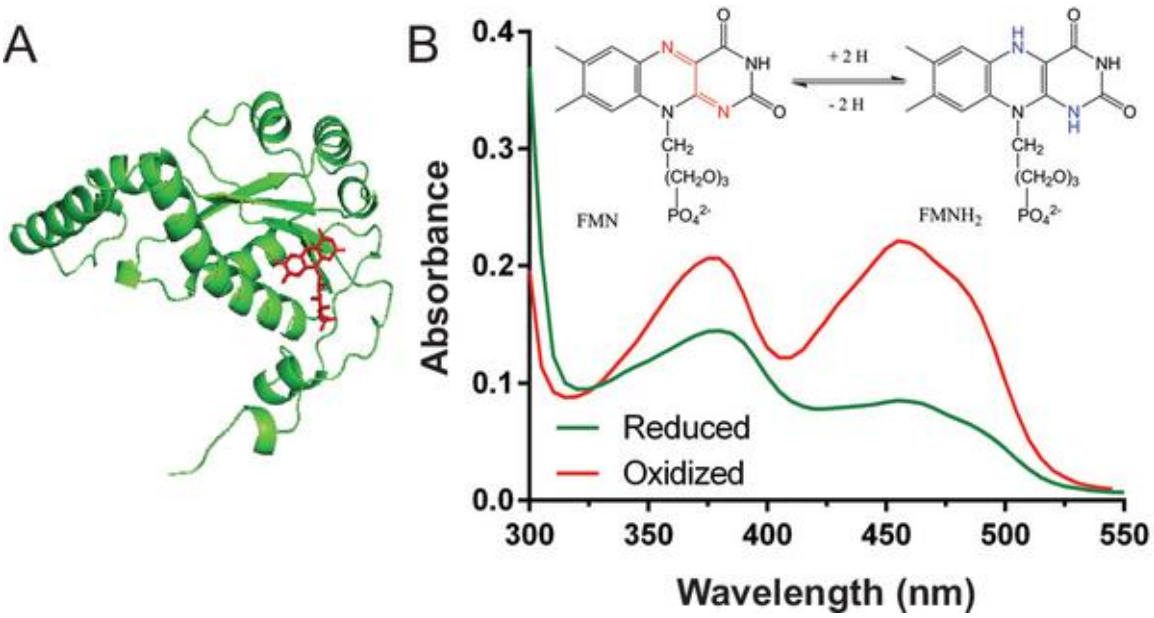

Figure 10. (A) An example crystal structure of a FMN-bound DI monomer (EC 1.6.99.1 or EC 1.6.99.3) (FMN is labelled in red) and (B) the decreased absorbance at 452 nm due to the reduction of FMN-DI to $FMNH_2$-DI. 20 μM FMN-DI was incubated with 20 μM NADH in 1 × TBS buffer (pH 7.4).

2.2. Materials and Methods

2.2.1. Materials

Solid Tris base, 10x Tris buffered saline (TBS) were purchased from Fisher Scientific (Waltham, MA). Reduced β-Nicotinamide adenine dinucleotide (NADH), reduced β-Nicotinamide adenine dinucleotide phosphate (NADPH), β-Nicotinamide adenine dinucleotide (NAD^+), Lactate Dehydrogenase from rabbit muscle (LDH), and sodium pyruvate were all purchased from Sigma Aldrich (St. Louis, MO). Thio-NAD^+, thio-NADH, and thio-NADP+ were all purchased from Oriental Yeast Company (Tokyo, Japan). Argon gas (Part #: AR 4.8OF-Q) was purchased from Praxair (Philadelphia, PA). Captair pyramid 2200 multi-function disposable glove box (size = XL) was purchased from Erlab (Rowley, MA).

2.2.2. Expression of Diaphorase

The procedures for enzyme expression and purification are similar as described previously.[54a] Briefly, the 636-bp DNA fragment encoding diaphorase (DI, GenBank accession number JQ040550) was expressed in *E.coli.* The DNA was amplified by PCR using the genomic DNA of G. stearothermophilus 10 as the template and two primers (forward primer: 50 -ACT TTA AGA AGG AGA TAT ACA TAT GAC GAA AGT ATT GTA CAT CAC CGC CC-30 ; reverse primer: 50 -AGT GGT GGT GGT GGT GGT GCT CGA GAA ACG TGT GCG CCA AGT CTT TCG CC-30). The recombinant GsDI (briefly called DI) was expressed in the plasmid pET20b-Gsdi, which was obtained using Simple Cloning.[56] The recombinant plasmids were transformed into *E. coli* BL21 Star (DE3). The expression of the recombinant protein was induced by adding isopropyl b-D-1- thiogalactopyranoside (IPTG) (0.1 mM final concentration). The cultures were

incubated at 18 °C for 16 h. The cells were harvested by centrifugation at 4 °C. The collected cells were disrupted by sonication, and the soluble target protein in the supernatant of the crude extract was purified using a Bio-Rad Profinity IMAC Ni-Charged Resin (Hercules, CA).[57] The purified FMN-DI concentration was determined by the molar extinction coefficient of bound FMN, which was ~ 12500 cm^{-1} M^{-1} at 455 nm.[58]

2.2.3. Preparation of Anaerobic Environment for Enzyme Assay

All sample preparations were performed in an argon-protected pyramid glove box. Solutions of enzymes, substrates and buffers, pipettes and 96-well plates were placed inside a pyramid glove box. The pyramid glove box was first fully filled with argon gas from the bottom, and then all the gas was purged out. The argon purging was repeated twice to ensure that air inside the box was mostly replaced with argon. The glove box was filled with argon gas and was well sealed. The buffer solutions were bubbled for ~ 20 min at ~ 20 psi with argon to remove dissolved oxygen immediately prior to the assay measurement. The 96-well plate was covered by an optically transparent lid, and sealed with vacuum grease (Dow Corning, MI) on the sides. After pipetting the sample solution, the sealed 96-well plate was transferred to a Cytation 3 Cell Imaging Multi-Mode Reader (Biotek, VT) for enzymatic assay.

2.2.4. Enzyme Assay

All enzyme assays were carried out using a Cytation 3 Cell Imaging Multi-Mode Reader (Biotek, VT). For reactions involving NAD(P)H, the absorbance at 340 nm was monitored in real time. Thio-modified analogues (thio-NAD^+/thio-$NADP^+$) were monitored at 400 nm. At least three replicates were tested in parallel. The rate of the

enzyme-catalyzed reaction was determined by fitting the initial velocity of curves, and the Michaelis-Menten constants were determined by fitting enzyme activities as a function of substrate concentrations, using the equation: $Y=V_{max}*X/(K_m+X)$, where Y is rate of the reaction, and X is the substrate concentration. All fittings were preformed using GraphPad Prism 6. The fitted V_{max} was converted to turnovers (s^{-1}) using a calibration curve.

2.3. Results and Discussion

2.3.1. Characterization of the FMN Reduction State under Anaerobic Conditions

The recombinant FMN-DI from *Geoba*cillus *stearothermophilus* was expressed in *E. coli* and purified as previously reported.[54a] As shown in **Figure 11**, a 20 μM solution of FMN-DI was first reduced to $FMNH_2$-DI by adding 20 μM NADH. In a regular aqueous solution containing dissolved oxygen, $FMNH_2$-DI was quickly oxidized back to FMN-DI with the simultaneous reduction of oxygen to H_2O_2, thus resulting in the increased absorbance at 452 nm. To stabilize the reduced state of $FMNH_2$-DI, dissolved oxygen was removed by purging the aqueous buffer solution with pure argon gas (20 psi, 30 min).[59] Under this anaerobic condition, $FMNH_2$-DI maintained a stable reduction state with a low absorbance at 452 nm. We hypothesized that FMN-DI, with the stabilized reduction state, might function as a transhydrogenase which catalyzes the hydride exchange between NADPH and NAD^+ (or vice versa). As shown in **Figure 12**, FMN-DI serves as a redox center to catalyze the reversible transfer of hydrides. To test this, analogues of thio-NAD^+ and thio-$NADP^+$ were used to characterize the transhydrogen reaction.[47a, 60]

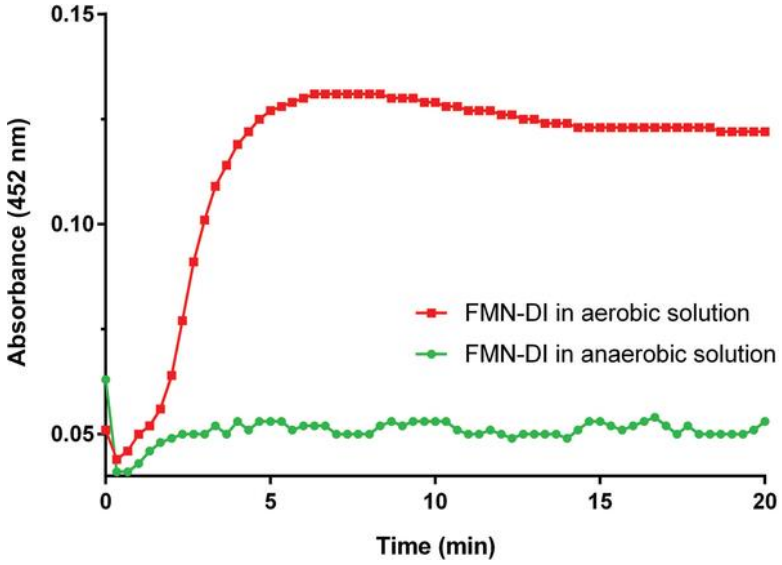

Figure 11. The oxidation state of FMN-DI in aerobic (red) and anaerobic (green) solution. To initiate the reduction state, 20 μM FMN-DI was first incubated with 20 μM NADH in 1 × TBS buffer (pH 7.4). The oxidation state of FMN-DI was monitored by the increased absorbance at 452 nm.

$$NADH + FMN\text{-}DI + H^{\oplus} \rightleftharpoons NAD^{\oplus} + FMNH_2\text{-}DI$$

$$FMNH_2\text{-}DI + NADP^{\oplus} \rightleftharpoons FMN\text{-}DI + NADPH + H^{\oplus}$$

Figure 12. Proposed mechanism of FMN-DI catalyzing the hydride transfer between NAD(H) and NADP(H).

2.3.2. Characterization of Transhydrogenase Activity Using a thio-NAD Analogue

As shown in **Figure 13A**, the thio-NAD^+ analogue resembles the structure of NAD^+, except for a thio-ester substitution at the nicotinamide group, which exhibits a red-shifted absorbance for reduced thio-NADH at ~ 400 nm. This shifted absorbance of thio-NADH is easily distinguishable from the 340 nm absorbance of NAD(P)H (**Figure**

13B). First, the substrate activity of the two analogues of thio-NAD^+ and thio-$NADP^+$ for FMN-DI were compared. It was found that thio-$NADP^+$ was much less active than thio-NAD^+ for FMN-DI (**Figure 14**). A further kinetics study showed that FMN-DI exhibited a much smaller k_{cat} for thio-$NADP^+$ than that for thio-NAD^+ (**Figures 15-16**). Thus only thio-NAD^+ was used as a reporter for characterizing the transhydrogen reaction. As shown in **Figure 13B**, the increased absorbance at 400 nm was observed for the DI-catalyzed transhydrogen reaction between NADH and thio-NAD^+, as well as between NADPH and thio-NAD^+. As a negative control, the incubation of thio-NAD^+ with NADH or NADPH did not result in a significant increase of absorbance at 400 nm. Another control experiment also showed that the addition of free FMN molecules could not enhance the rate of the transhydrogen reaction (**Figures 19-21**). All of these results suggested that the DI-bound FMN cofactor was responsible for catalyzing the transhydrogen reaction, not the unbound and freely diffused FMN. FMN-DI was further found to discriminate between NADH and NADPH, which catalyzed the reaction between NADH and thio-NAD^+ 3-fold faster than the reaction between NADPH and thio-NAD^+. Detailed kinetic analysis showed that FMN-DI exhibited similar turnover numbers between NADH (a k_{cat} value of ~ 1.64 ± 0.05 s^{-1}) and NADPH (a k_{cat} value of ~ 1.93 ± 0.06 s^{-1}). However, the apparent K_m value of NADH (~ 24 ± 3 μM) was much smaller than that of NADPH (~ 699 ± 49 μM) (**Figure 12C**). This suggested that NADPH was bound to the enzyme less efficiently than NADH. Thus FMN-DI might favor the hydride transfer from a high concentration of NADPH to a low concentration of NAD^+. Detailed activity curves are shown in **Figures 21-22**.

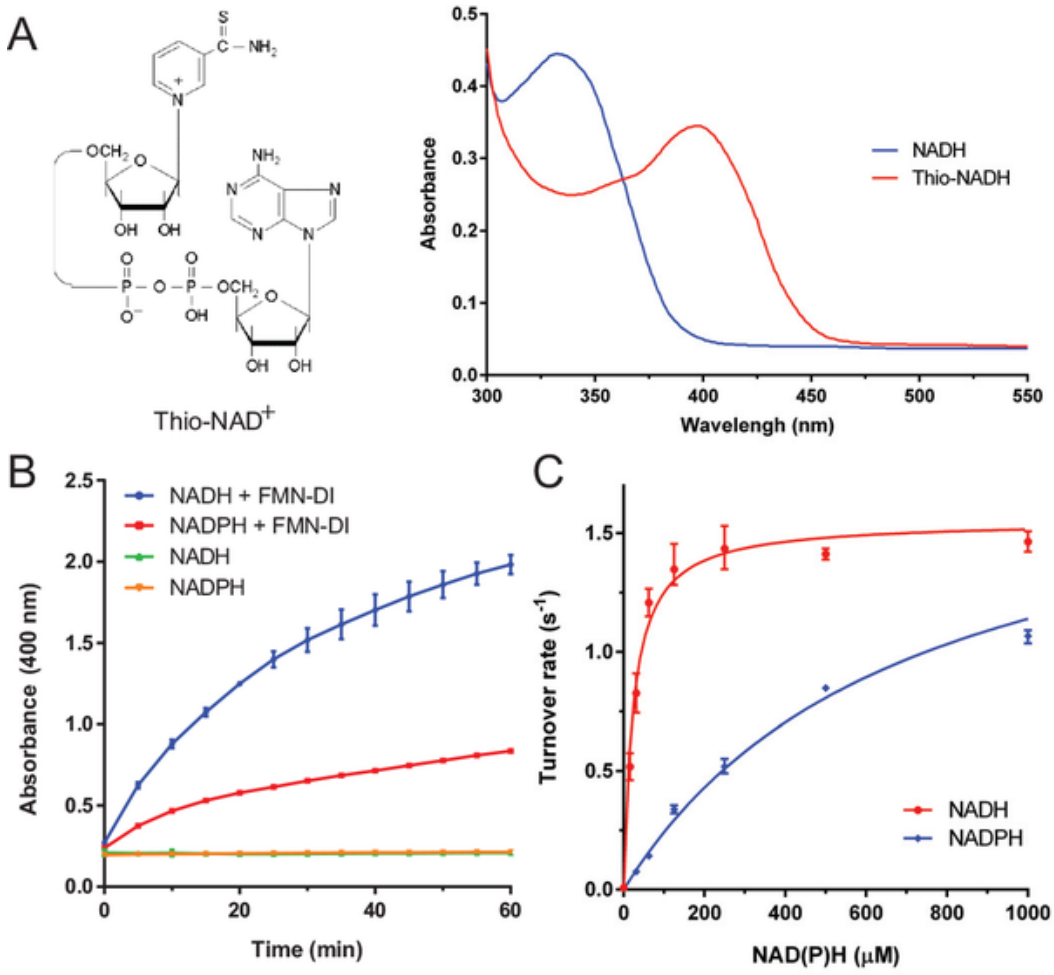

Figure 13. Characterization of the transhydrogenase activity of FMN-DI. (A) A thio-NAD^+ analogue (left) and a red-shifted maximum absorbance at ~ 400 nm for a reduced thio-NADH (right). (B) The hydride transfer from NAD(P)H to thio-NAD^+ with the increased absorbance at 400 nm. Condition: 500 nM FMN-DI was incubated with 500 μM thio-NAD^+ and 500 μM NAD(P)H in 1 × TBS buffer (pH 7.4) at room temperature. (C) The Michaelis-Menten fitting of NAD(P)H concentrations for the DI-catalyzed transhydrogen reaction. Error bars were generated as the range of at least three replicates.

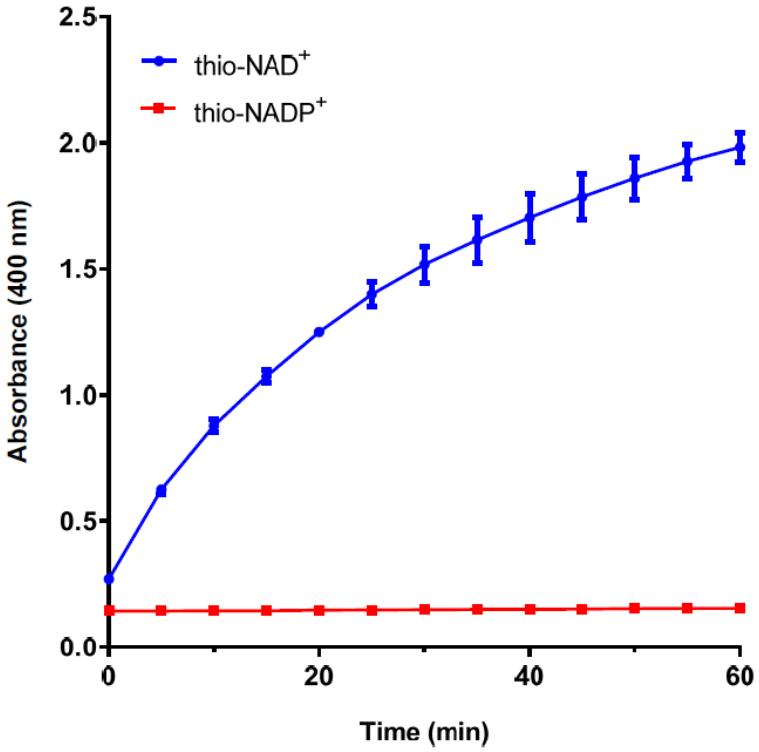

Figure 14. Substrate activity of thio-NAD+ and thio-NADP+ for a FMN-DI. A hydride transfer between NADH and thio-NAD(P)+ was monitored by an increased absorbance at 400 nm. Conditions: 500 nM DI was added into a solution containing 500 μM NADH and either 500 μM thio-NAD+ (blue) or thio-NADP+ (red) in 1 × TBS (pH 7.4) at room temperature. The thio- NADP+ was found to have almost no activity with a FMN-DI. Error bars were generated as the range of at least three replicates.

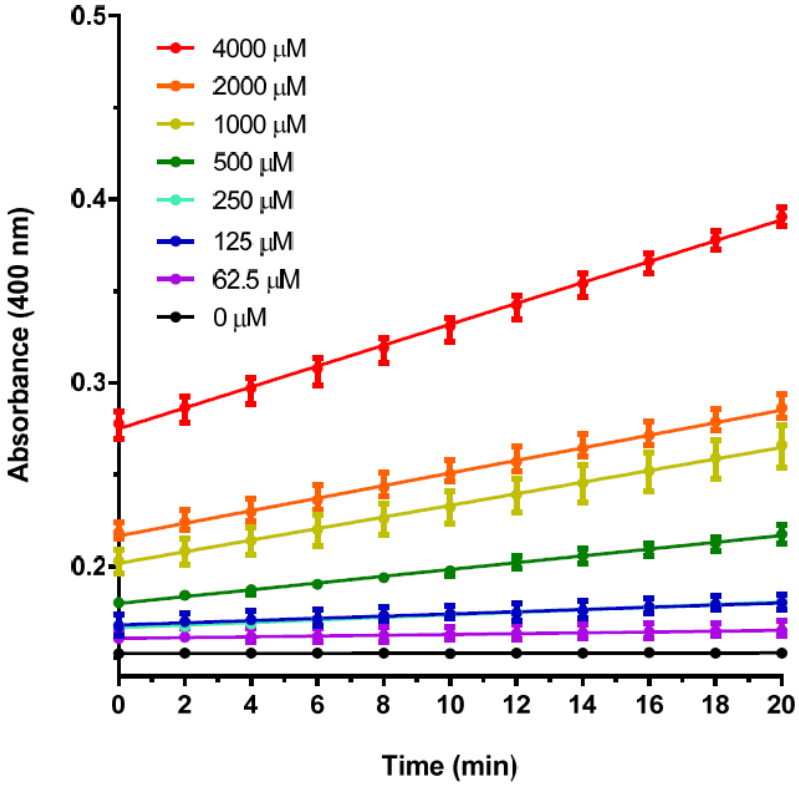

Figure 15. Raw activity curves of titrating the concentration of thio-NAD+. The hydride transfer between NADH and thio-NAD+ was monitored by the increased absorbance at 400 nm. Conditions: 2 mM NADH and 25 nM DI were incubated with a set of thio-NAD+ concentrations varied from 62.5 µM to 4000 µM, in pH 7.4, 1 × TBS buffer at room temperature. Error bars were generated as the range of at least three replicates.

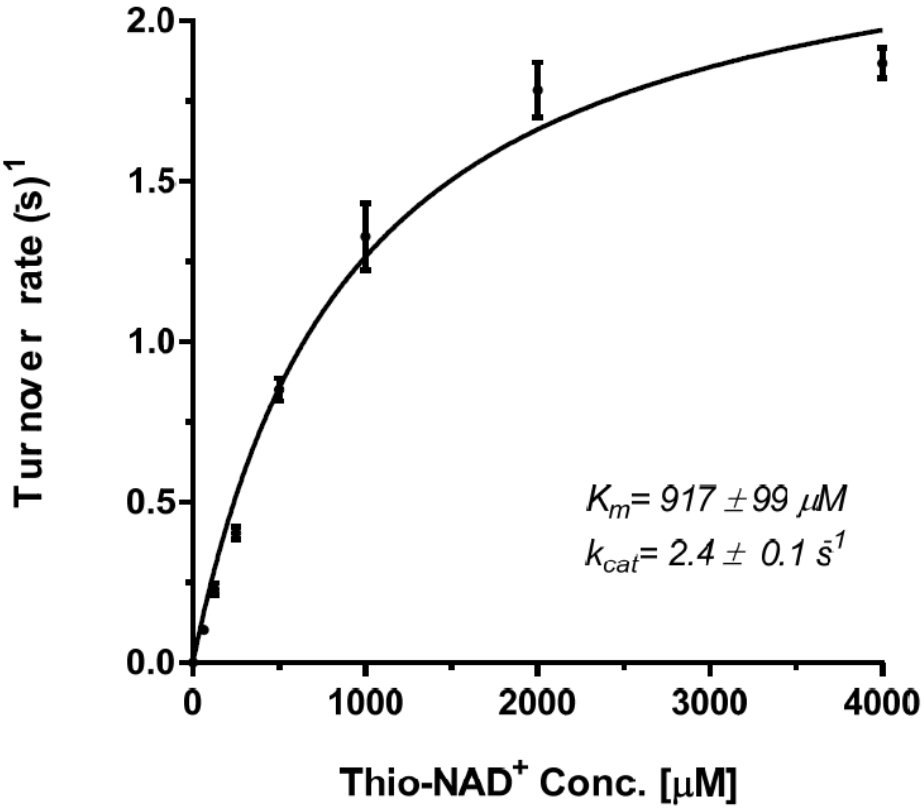

Figure 16. The Michaelis-Menten fitting of thio-NAD+ concentrations for the DI-catalyzed transhydrogen reaction. Error bars were generated as the range of at least three replicates.

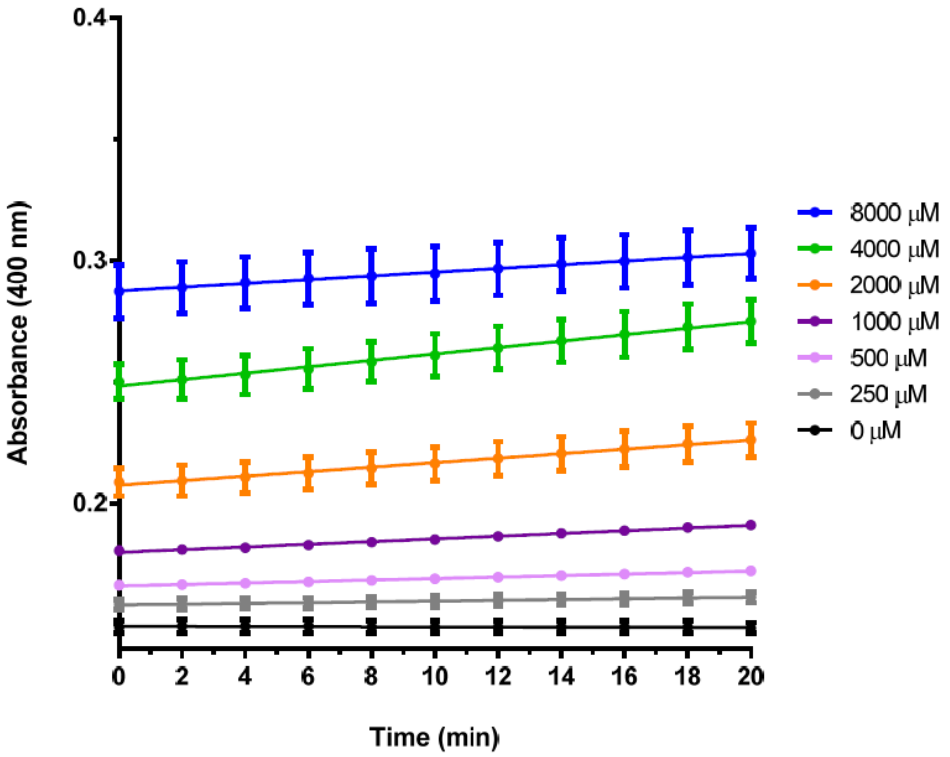

Figure 17. Raw activity curves of titrating the concentration of thio-NADP+. The hydride transfer between NADH and thio-NADP+ was monitored by the increased absorbance at 400 nm. Conditions: 2 mM NADH and 100 nM DI were incubated with a set of thio-NADP+ concentrations varied from 250 µM to 8000 µM, in pH 7.4, 1 × TBS buffer at room temperature. Error bars were generated as the range of at least three replicates. Thio-NADP+ poorly reacted with FMN-DI, with clearly observed activities for the concentrations > 1000 µM. Substrate inhibition also happened for thio-NADP+ at 8000 µM or above.

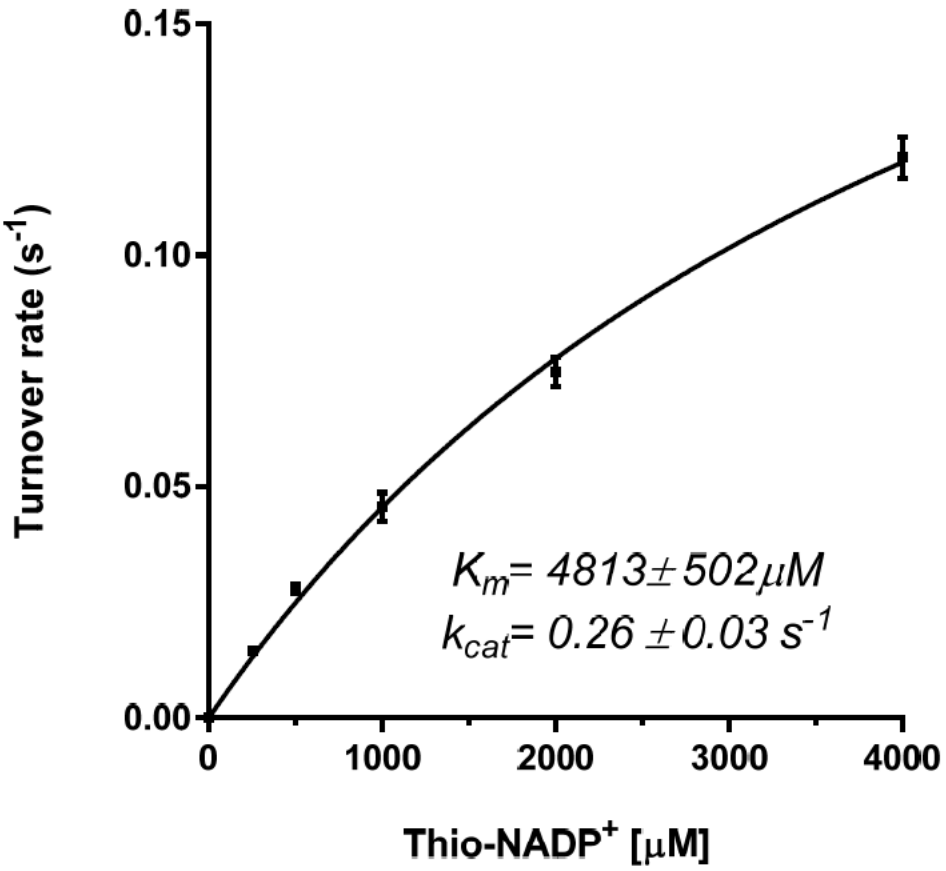

Figure 18. The Michaelis-Menten fitting of thio-NADP+ concentrations for the DI-catalyzed transhydrogen reaction. Error bars were generated as the range of at least three replicates.

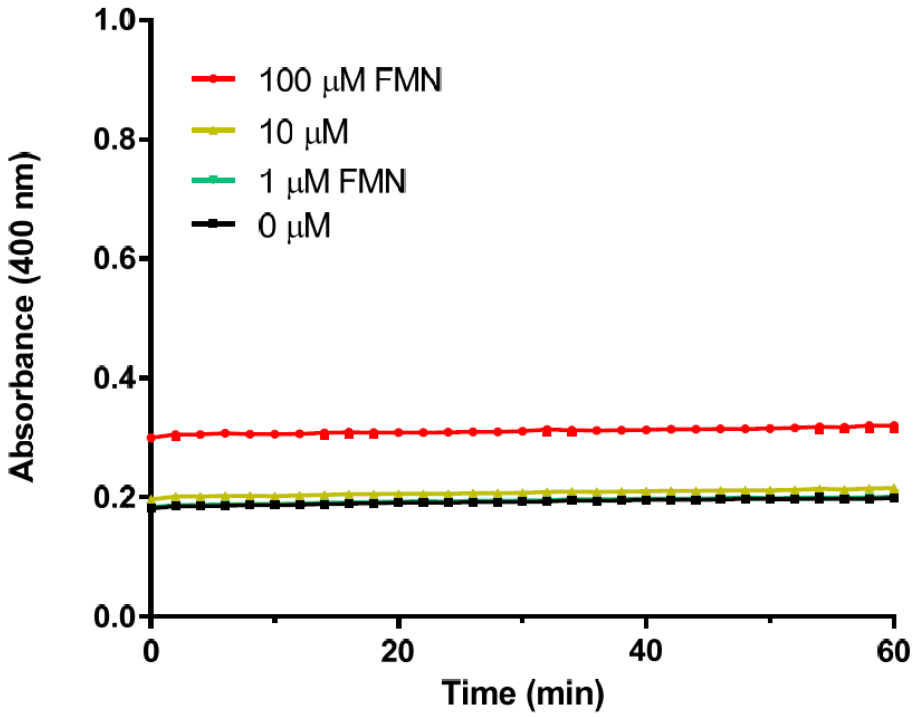

Figure 19. The addition of free FMN molecules does not significantly catalyze the transhydrogen reaction between a NADH and a thio-NAD+. Condition: FMN from 1 μM to 100 μM was added into a solution containing 1 mM NADH and 1 mM thio-NAD+ in pH 7.4, 1 × TBS at room temperature. The slopes of all curves were similar. Error bars were generated as the range of at least three replicates.

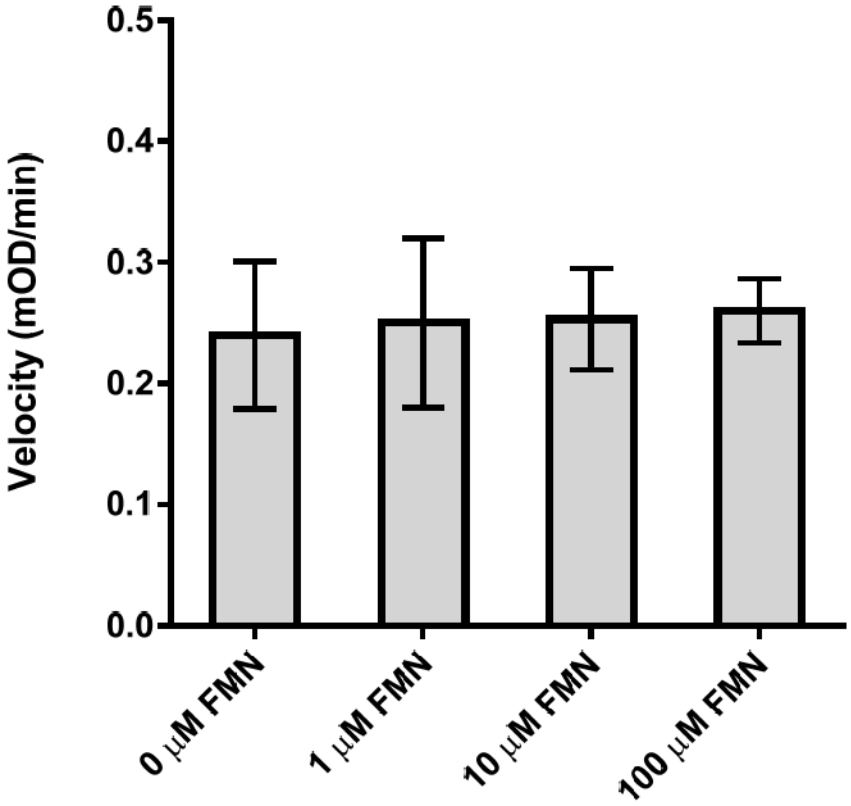

Figure 20. The slopes of reaction curves containing 0, 1, 10 and 100 μM FMN were similar. This indicates that the addition of free FMN molecules does not significantly catalyze the transhydrogen reaction between a NADH and a thio-NAD+. Error bars were generated as the range of at least three replicates.

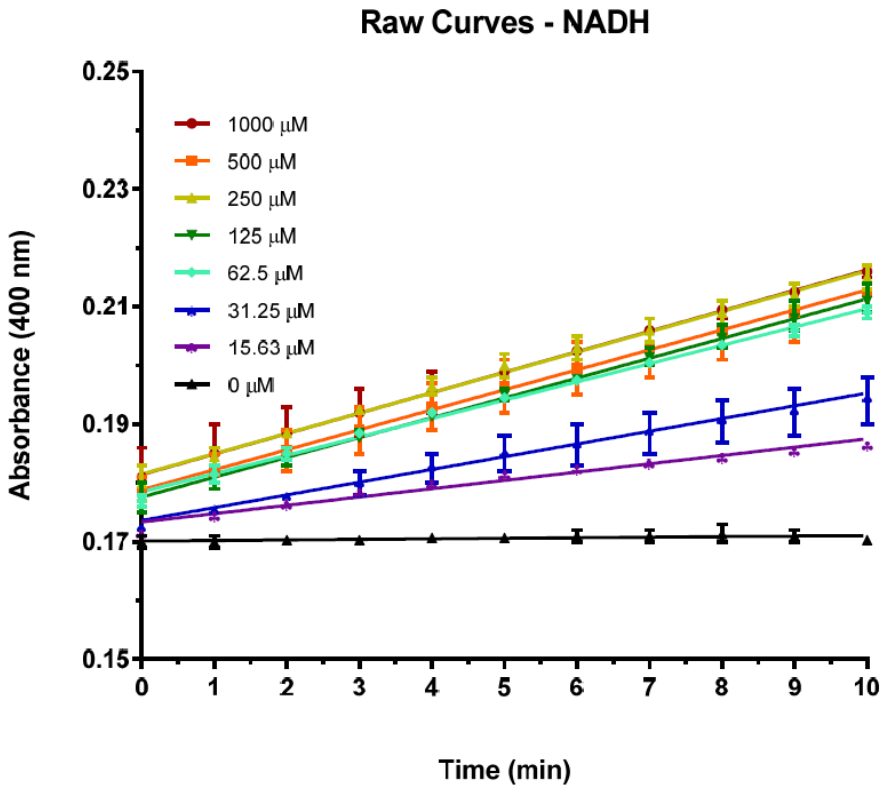

Figure 21. Raw curves used for Michaelis-Menten kinetic fitting of the *Km* and *kcat* values for NADH. The hydride transfer between NADH and thio-NAD+ was monitored by the increased absorbance at 400 nm. Initial velocities were determined by fitting the linear range of the beginning 5-10 minutes of the reaction. Conditions: 2 mM thio-NAD+ and 25 nM DI were incubated with a set of NADH concentrations varied from 15 µM to 1000 µM, in pH 7.4, 1 × TBS buffer at room temperature. Error bars were generated as the range of at least three replicates.

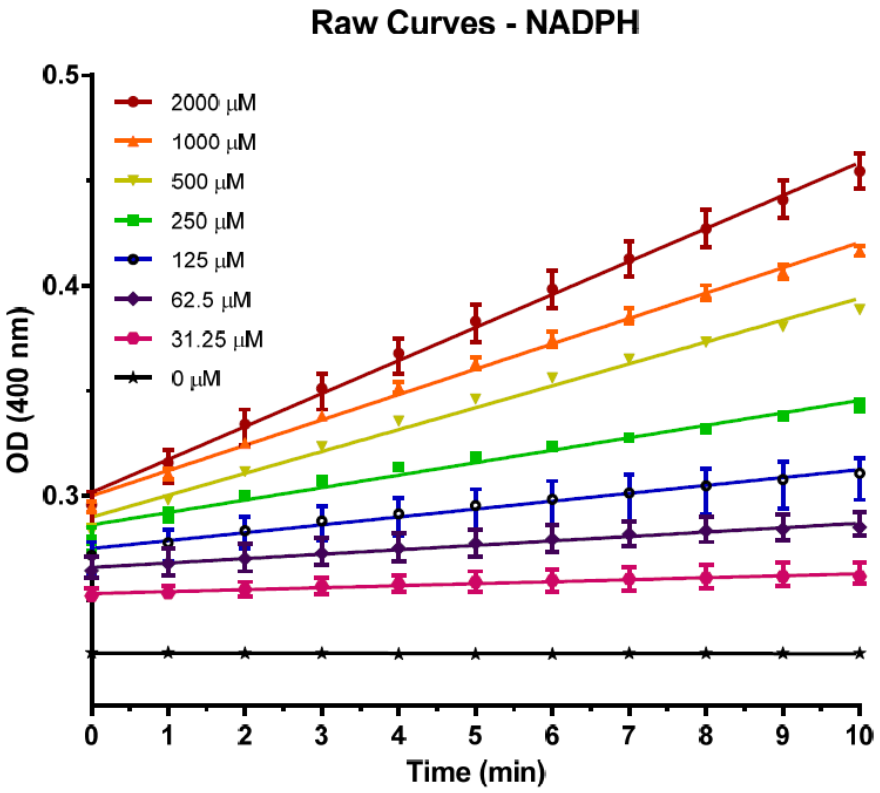

Figure 22. Raw curves used for Michaelis-Menten kinetic fitting of the *Km* and *kcat* values for NADPH. The hydride transfer between NADPH and thio-NAD+ was monitored by the increased absorbance at 400 nm. Initial velocities were determined by fitting the linear range of the beginning 5-10 minutes of the reaction. Conditions: 2 mM thio-NAD+ and 100 nM DI were incubated with a set of NADPH concentrations varied from 31 µM to 2000 µM, in pH 7.4, 1 × TBS buffer at room temperature. Error bars were generated as the range of at least three replicates.

2.3.3. Demonstration of the Transhydrogenase Activity of Diaphorase Using an Enzyme Cascade

Using this newly discovered transhydrogenase activity, FMN-DI was demonstrated to allow a NADH-specific lactate dehydrogenase to utilize NADPH as an electron donor, where NADPH was converted to NADH by the DI-catalyzed transhydrogen reaction (**Figure 23)**. A special lactate dehydrogenase (LDH) was chosen that reacted with NADH 100-fold faster than NADPH for converting pyruvate to lactate (**Figure 24**). As shown in **Figure 25A**, a mixture of NADPH and thio-NAD^+, where the DI-catalyzed hydride exchange from NADPH to thio-NAD^+, was first used to generate thio-NADH, accompanied by an increased absorbance at 400 nm. The sequential addition of LDH induced a quick decrease in the absorbance at 400 nm, indicating the consumption of thio-NADH by LDH. Next, FMN-DI was tested for catalyzing the direct hydride transfer between NADPH and NAD^+. As shown in **Figure 25B**, LDH cannot efficiently use NADPH as an electron donor without the addition of FMN-DI, resulting in a very slow decrease in the absorbance at 340 nm (shown in red). Conversely, the addition of FMN-DI into the reaction mixture catalyzed the hydride transfer from NADPH to NAD^+ with the production of more NADH. Then, the produced NADH was quickly consumed by the LDH with a faster decreased absorbance at 340 nm (shown in black). As another control experiment, FMN-DI was incubated with the mixture of NADPH and NAD^+ without the addition of LDH to consume the produced NADH (shown in green). The absorbance at 340 nm varied slightly over time which was similar to that of the no-enzyme control (shown in blue) because both reduced NADH and NADPH had similar absorbance at 340 nm. Similarly, FMN-DI was also demonstrated to

activate a NADH-specific malic dehydrogenase to utilize NADPH for reducing oxaloacetate (**Figures 26-28**). The above results demonstrated that FMN-DI catalyzed the hydride exchange between NADPH and NAD^+ under anaerobic conditions. Most natural transhydrogenase's in living cells under reduced environments favor the transhydrogenation from NADPH to NADH, mainly due to the fact that the physiological ratio of NADPH/$NADP^+$ (~ 60) is much higher than the ratio of NADH/NAD^+ (~ 0.03),[45, 47a] and the cellular concentration of NADPH (~ 120 μM) is also higher than that of NADH (~ 80 μM).[61] This study implied that DI could have a new function as transhydrogenase for some organisms, especially for anaerobic species.

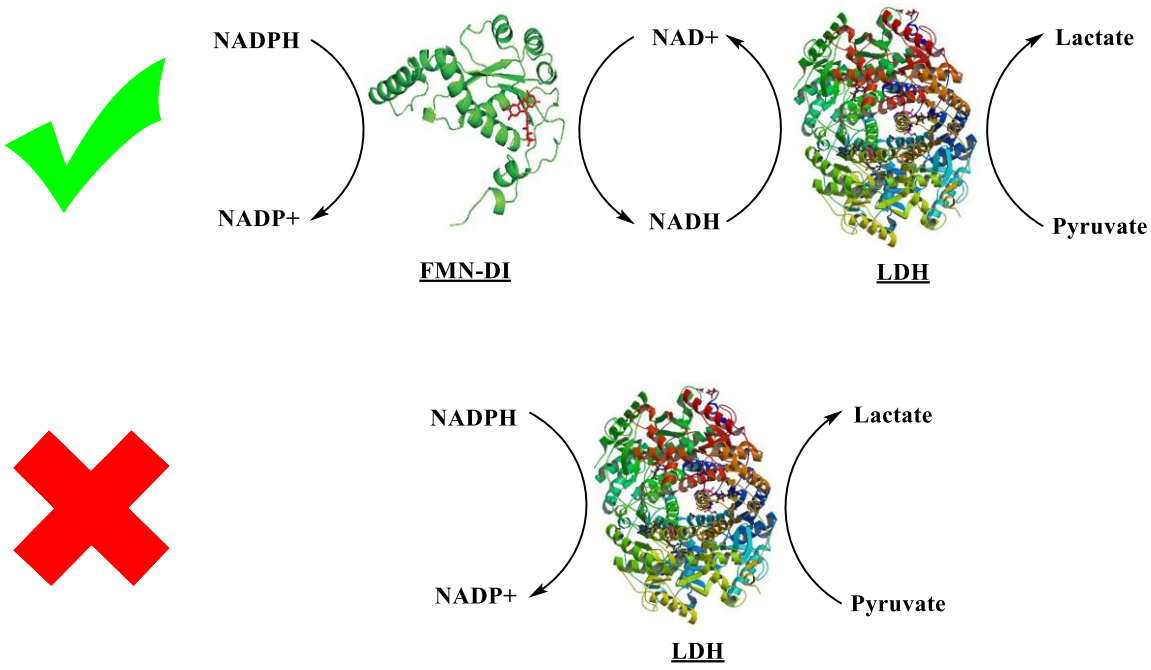

Figure 23. Enzyme cascade demonstrating the DI catalyzed transhydrogen reaction. DI first generates NADH from NADPH. NADH is then consumed by LDH (or MDH) to oxidize NADH to NAD+. NADPH cannot be consumed by LDH (or MDH).

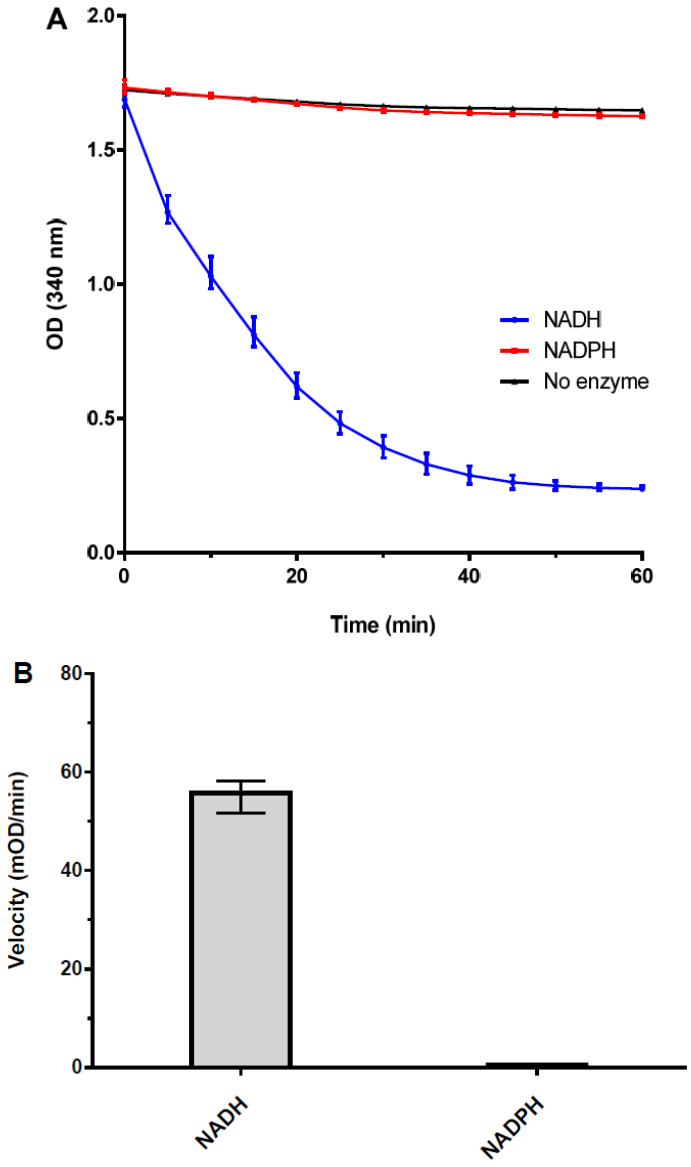

Figure 24. Activity of LDH toward NADH and NADPH. (A) Raw activity curves for comparing the activity of LDH for NADH and NADPH. (B) The LDH-catalyzed oxidation velocity of NADH and NADPH: 1 nM LDH was added to the substrate solution of 1 mM NAD(P)H and 1 mM Pyruvate at room temperature in pH 7.4, 1×TBS buffer. Error bars were generated as the range of at least three replicates.

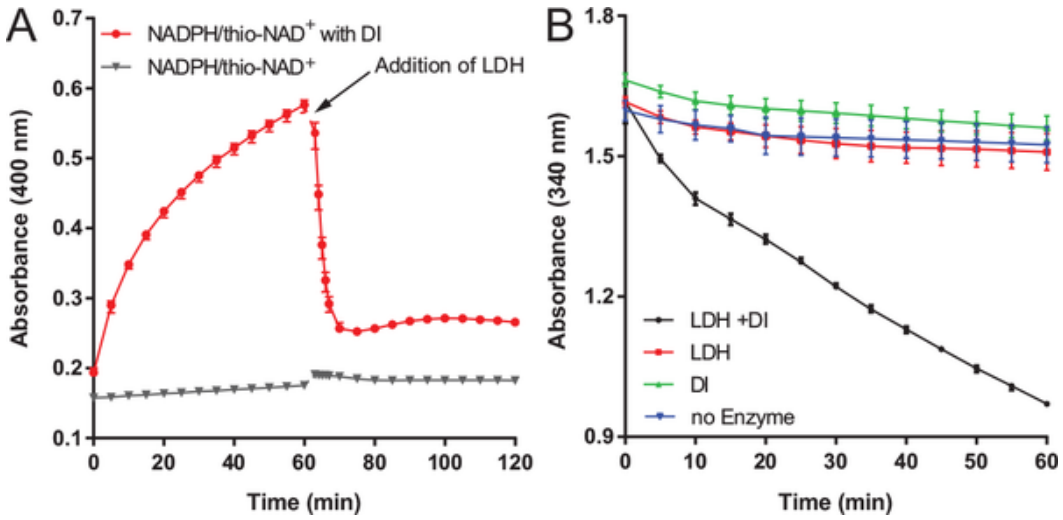

Figure 25. (A) Real-time monitoring of the hydride exchange from NADPH to thio-NAD^+ at 400 nm, and the consumption of thio-NADH with the addition of LDH. Condition: 1 mM NADPH and 1 mM thio-NAD^+ were first incubated with 500 nM FMN-DI in 1 × TBS buffer (pH 7.4) at room temperature. Then 10 nM LDH and 1 mM pyruvate were added to oxidize thio-NADH. (B) The LDH-catalyzed oxidation was activated by the addition of a FMN-DI to convert NADPH to NADH (black) and controls of no addition of DI (red), no addition of LDH (red) and no addition of enzymes (blue). Condition: 1 mM NADPH and 1 mM NAD^+ were first incubated with or without 1 μM FMN-DI for one hour in 1 × TBS buffer (pH 7.4). Then 1 nM LDH and 1 mM pyruvate were added to evaluate the oxidation of the mixture of NADPH and NAD^+. Anaerobic solution was used for the assay. Error bars were generated as the range of at least three replicates.

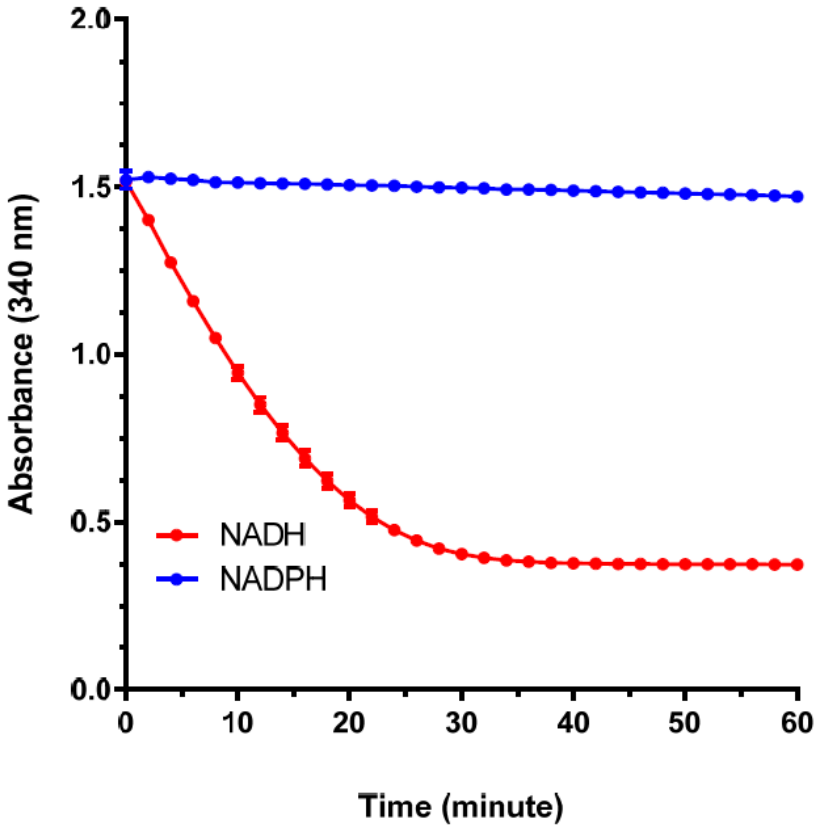

Figure 26. Raw activity curves for comparing the activity of MDH for NADH and NADPH. Running conditions: 20 nM MDH was added to the substrate solution of 1 mM NAD(P)H and 1 mM oxaloacetate at room temperature in pH 7.4, 1×TBS buffer. Error bars were generated as the range of at least three replicates.

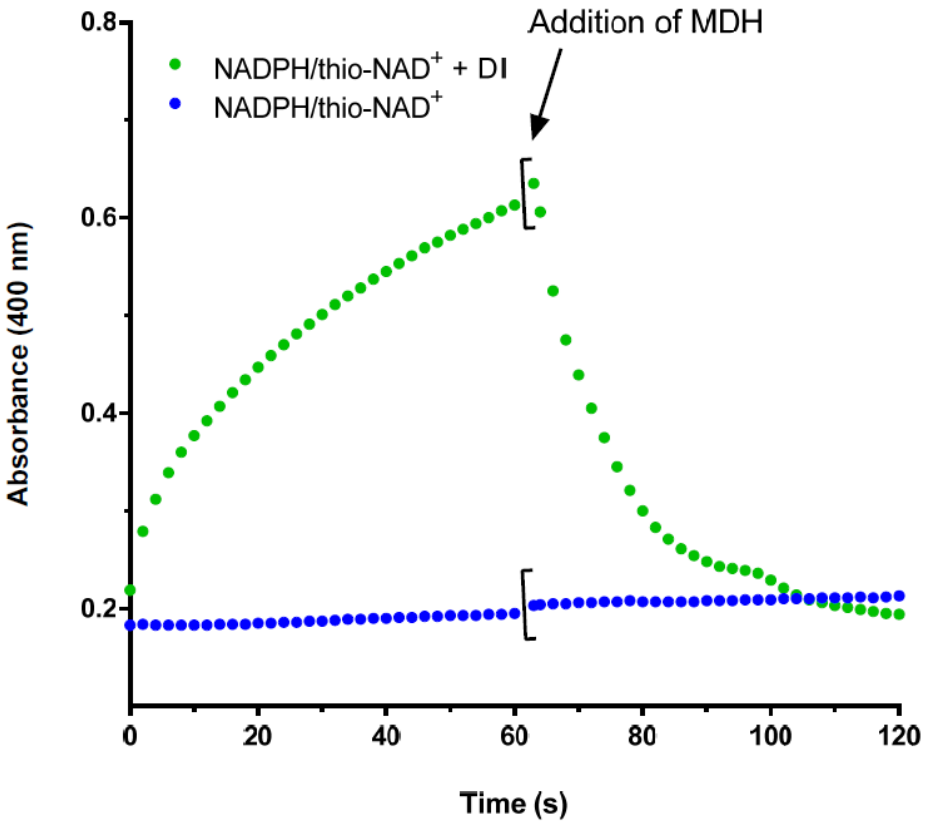

Figure 27. Real-time monitoring of the hydride exchange from NADPH to thio-NAD+ at 400 nm, and the consumption of thio-NADH with the addition of MDH. Condition: 1 mM NADPH and 1 mM thio-NAD+ were first incubated with 500 nM FMN-DI in 1 × TBS buffer (pH 7.4) at room temperature. Then 100 nM MDH and 1 mM oxaloacetate were added to oxidize thio-NADH.

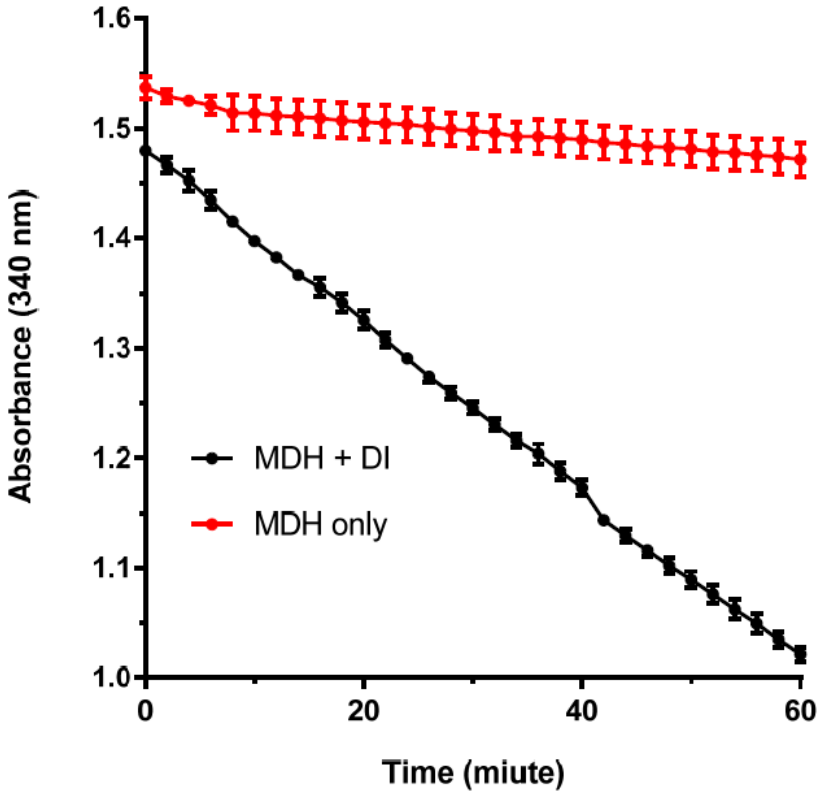

Figure 28. The MDH-catalyzed oxidation was activated by the addition of a FMN-DI to convert NADPH to NADH (black) and controls of no addition of DI (red). Condition: 1 mM NADPH and 1 mM NAD+ were first incubated with or without 500 nM FMN-DI for one hour in 1 × TBS buffer (pH 7.4). Then 100 nM MDH and 1 mM oxaloacetate were added to evaluate the oxidation of the mixture of NADPH and NAD+. Anaerobic solution was used for the assay. Error bars were generated as the range of at least three replicates.

2.4. Conclusion

In summary, a novel transhydrogenase activity of FMN-DI was discovered by stabilizing the reduced state of $FMNH_2$ under anaerobic conditions. FMN-DI was demonstrated to catalyze the hydride transfer between NADPH and NAD^+. In the future, it may be possible to incorporate this FMN-DI into synthetic enzymatic pathways for balancing NADH generation and NADPH consumption for anaerobic production of biofuels and biochemicals.

2.5. Acknowledgements

This chapter resulted in a publication published in PLOS One.[62] The following authors contributed to this work: John Collins, Ting Zhang, Scott Huston, Fangfang Sun, Y.-H. Percival Zhang, and Jinglin Fu.

Chapter 3

An Activity Transition from NADH Dehydrogenase to NADH Oxidase during Protein Denaturation

Abstract

A decrease in the specific activity of an enzyme is commonly observed when the enzyme is inappropriately handled or is stored over an extended period. Here, a functional transition of a FMN-bound diaphorase (FMN-DI) that happened during the long-term storage process is reported. It was found that FMN-DI did not simply lose its NADH dehydrogenase activity after a long-time storage, but obtained a new enzyme activity of NADH oxidase. Further mechanistic studies suggested that the alteration of the binding strength of a FMN cofactor with a DI protein could be responsible for this functional switch of the enzyme.

3.1. Introduction

Protein denaturation is commonly observed during long-term storage due to environmental stress, such as elevated temperature, extreme pH or solvent impact.[63] This process is often associated with multi-level conformational changes including unfolding of polypeptide chains, dissociation of multimeric complexes/protein-cofactor interactions, formation of aggregates, as well as oxidative damage of amino acid residues and cofactors. Enzyme function can be significantly decreased or even completely lost as a result of denaturation. Many studies have reported detailed kinetics of protein denaturation and their unfolding processes by increasing temperature, changing pH, or adding chemical denaturants such as urea.[63a, 64] Solvents have also been suggested to play a key role in protein stability and denaturation.[65] For example, multiple studies have reported that an ordered hydrogen-bonded water environment favors protein stability and activity by stabilizing the hydrophobic interactions of a folded protein.[66] Small molecules such as Trimethylamine N-Oxide (TMAO) that form hydrogen bonds with water can serve as protein-stabilizing reagents.[67] Conversely, urea denatures proteins by hydrogen bonding with polypeptide chains and disrupting internal hydrogen bonds between amino acids, as well as excluding internal water bound to proteins. Ionic liquids have also been widely studied for affecting protein folding and stability,[68] which broadens the potential applications of proteins in non-aqueous environments.[69]

The degradation of proteins may also enhance or induce new catalytic activities. For example, a protease-digested fragment (microperoxidase-11) of a protein cytochrome c was found to be 100-fold more active as a peroxidase than a native protein, possibly due to the exposure of the heme cofactor to the solvent in the peptide fragment.[70]

Diaphorase (DI) is commonly used as a NAD(P)H dehydrogenase that catalyzes the electron transfer from NAD(P)H to a variety of electron acceptors, such as methylene blue,[71] resazurin,[49] vitamin K_3[50] and dichlorophenolindophenol (**Figure 29A**).[55] The redox center of a DI protein is a bound flavin monucleotide (FMN) that accepts two electrons from NADH, and is reduced to $FMNH_2$ (**Figure 29B**). The reduction of FMN-DI to $FMNH_2$-DI can be characterized by the reduced absorbance at ~ 452 nm (**Figure 29C**). FMN-containing DI was also reported to behave as a NADH oxidase where the reduced $FMNH_2$-DI was oxidized by molecular oxygen to produce hydrogen peroxide. However, few reports have carefully studied how the dehydrogenase activity was correlated to the oxidase activity for FMN-DI. Here, a transformed activity of a FMN-bound DI from a primary dehydrogenase to a primary oxidase that happened during the storage denaturation of protein is reported. The alteration of the binding strength of the FMN cofactor to the DI protein was suggested to be responsible for the observed functional switch of the enzyme.

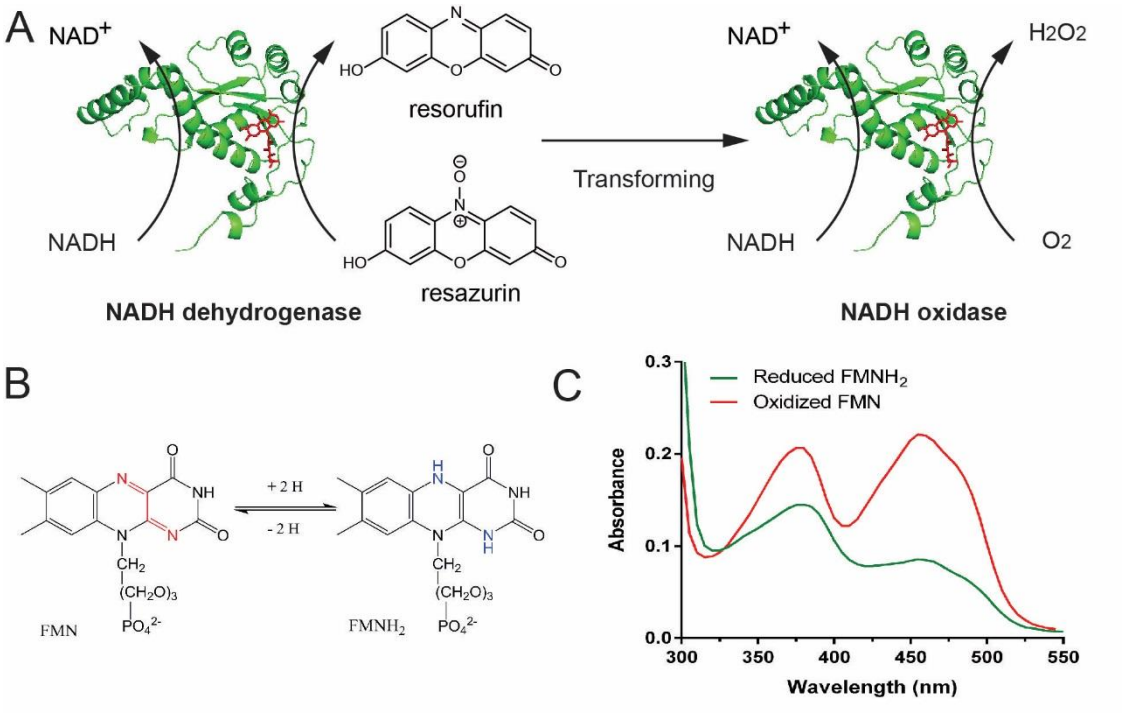

Figure 29. (A) Schematic illustration of the transformed activity of a FMN-DI from a NADH dehydrogenase to a NADH oxidase during the denaturation. (B) The redox center of a FMN cofactor accepts two electrons for reducing to a $FMNH_2$. (C) The decreased absorbance at 455 nm due to the reduction of FMN-DI to $FMNH_2$-DI.

3.2. Materials and Methods

3.2.1 Materials

β-nicotinamide adenine diphosphate (NAD^+), reduced β-nicotinamide adenine diphosphate (NADH), resazurin, flavin mononucleoide (FMN), sodium phosphate and HEPES sodium salt were all purchased from Sigma-Aldrich (St. Louis, MO). Amplex Red, hydrogen peroxide and 10 × Tris Buffer Saline (TBS) were purchased from Fisher Scientific. Argon gas (Part #: AR 4.8OF-Q) was purchased from Praxair (Philadelphia, PA). Captair pyramid 2200 multi-function disposable glove box (size = XL) was purchased from Erlab (Rowley, MA).

3.2.2 Expression of Diaphorase

The procedures of the expression and purification of a thermophilic DI has been described elsewhere.[54a, 62] Briefly, a 636-bp DNA fragment encoding diaphorase (DI, GenBank accession number JQ040550) was expressed in *E. coli* BL21(DE3). The DNA fragment was amplified by PCR using the genomic DNA of *Geobacillus stearothermophilus* 10 (Gs10) as the template and two primers (forward primer: 50 -ACT TTA AGA AGG AGA TAT ACA TAT GAC GAA AGT ATT GTA CAT CAC CGC CC-30 ; reverse primer: 50 -AGT GGT GGT GGT GGT GGT GCT CGA GAA ACG TGT GCG CCA AGT CTT TCG CC-30). The PCR product was inserted into plasmid pET by using Simple Cloning.[56] After transforming into *E. coli* BL21 Star (DE3), the expression of the protein was induced by adding isopropyl β-D-1- thiogalactopyranoside (IPTG) (0.1 mM final concentration). The cell cultures were incubated at 18 °C for 16 h, and then the cells were harvested by centrifugation at 4 °C. The collected cells were disrupted by sonication, and the soluble target protein in the supernatant of the crude

extract was mixed with excess FMN followed by affinity adsorption on a Bio-Rad Profinity IMAC Ni-charged resins (Hercules, CA).[57] The concentration of the eluted FMN-DI from resins was determined by the molar extinction coefficient of the bound FMN (~12500 cm^{-1} M^{-1} at 455 nm). [58] The monomeric DI protein concentration was determined by the extinction coefficient of the polypeptide chain: ~ 24810 cm^{-1} M^{-1} at 280 nm.

3.2.3. Preparation of Anaerobic Buffers

The procedure was similar to what was published previously.[62] Briefly, all solutions were prepared in an argon-protected pyramid glove box. The pyramid glove box was filled with argon gas and was well sealed. The buffer solutions were bubbled for ~ 20 min at ~ 20 psi with argon to remove dissolved oxygen immediately prior to the assay measurement. The 96-well plate was covered by an optically transparent lid, and sealed with vacuum grease (Dow Corning, MI) on the sides.

3.2.4. Molecular Weight-Cutoff Filtration

Amicon 3 kD-0.5 mL filter was used for the filtration. ~ 90 μM, 100 μL FMN-DI solution was added onto the top of the filter, followed by the addition of ~ 400 μL HEPES buffer. The filter was then placed inside an Eppendorf 5424 R centrifuge with 10, 000 rpm for 30 mins at 4 °C. The protein solution was then re-quantified to ~ 100 μL for measuring their absorbance with Nanodrop or Biophotometer (Eppendorf).

3.2.5. Enzyme Assay and Fitting

All enzyme and substrate solutions were prepared in pH 7.4, 1 × Tris Buffered Saline (TBS). Enzyme assays were performed using a Cytation 3 Cell Imaging Multi-Mode Reader (Biotek, VT). For reactions involving NADH, the absorbance at 340 nm was monitored in real time. Fluorescence assays involving resazurin and Amplex Red were monitored with excitation at ~ 532 nm and emission at ~ 590 nm. At least three replicates were tested in parallel. The rates of the enzyme-catalyzed reaction were determined by the initial velocity with fitting linear range at the beginning of the reaction. For FMN titration experiments, the control reaction rates of free FMN-catalyzed reactions were subtracted from the measured values of DI-catalyzed reactions. The apparent dissociation constant (K_d) for FMN binding to DI protein was determined by fitting the increased enzyme activity as a function of the addition of excess free FMN molecules, using the equation of "One site – Total binding": $Y = B_{max} * X/(K_d + X) + Background$; where Y is the rate of DI-catalyzed reaction, X is the FMN concentration, *Background* is the rate of DI-catalyzed reaction without the addition of excess free FMN. All fittings were performed using GraphPad Prism 6.

3.2.6. Circular Dichroism

All samples were prepared in pH 7.5, 20 mM sodium phosphate buffer. Circular dichroism (CD) spectra were recorded with a Jasco J-810 spectropolarimeter. Spectra were measured at 25 °C in quartz cuvettes. For each spectrum, 3 scans were averaged together.

3.3. Results and Discussion

3.3.1 Observation of Increased NADH Oxidase Activity by the Storage Denaturation of Protein

To characterize the NADH dehydrogenase activity of DI from *G. stearothermophilus*, a resazurin assay was used, in which FMN-DI catalyzed the oxidation of NADH to NAD^+ while concurrently transferring two electrons to resazurin for reducing it to the strongly fluorescent resorufin.[72] Freshly-made FMN-DI showed a much higher dehydrogenase activity (>20-fold) than the aged FMN-DI solution that has been frequently used and stored at 4 °C for more than a year (**Figure 30A**). This decreased activity was also commonly observed for many other proteins during their storage, which could be induced by a series of factors, such as folding change, aggregation, oxidation, and cofactor damage. However, it was accidentally discovered that as FMN-DI lost its dehydrogenase activity, it became more active as a NADH oxidase, which used NADH to reduce O_2 to H_2O_2. As shown in **Figure 30B**, the NADH oxidation was characterized by the decreased absorbance at 340 nm. The old FMN-DI solution catalyzed the complete depletion of NADH within 50 minutes, whereas the freshly-made FMN-DI solution showed very little oxidation of NADH with only slight decreased absorbance at 340 nm. In **Figure 30C**, the production of H_2O_2 during the NADH oxidation was verified by adding horseradish peroxidase (HRP) that used produced H_2O_2 to oxidize Amplex Red to strongly fluorescent resorufin. The formation of C4a-hydroperoxyflavin from the oxidation of reduced FMN is suggested as a key intermediate for producing H_2O_2 according to previous studies.[73] FMN-DI was also tested for any potential NADH peroxidase activity that could use NADH to reduce H_2O_2. This

was performed under anaerobic conditions in which the oxidase activity was inhibited.[74] Different concentrations of FMN-DI solutions from 50 nM to 400 nM were incubated with NADH and H_2O_2. FMN-DI solutions were not observed to have any significant NADH peroxidase activity as compared with the no enzyme solution (**Figure 31**). In **Figure 30D**, FMN-DI solution was tested for the transformation from a NADH dehydrogenase to a NADH oxidase activity by incubation at room temperature over a period of seven days. As expected, for the fresh FMN-DI solution (day 0), a strong dehydrogenase activity was observed, and the oxidase activity was very weak. As the enzyme solution was incubated over a period of several days, the oxidase activity increased accordingly. Conversely, the dehydrogenase activity decreased as more days passed (**Figures 32-33**). As a control, free FMN molecules showed very little oxidase activity at even high micro-molar concentrations (**Figure 34**). This result suggested that a FMN-containing DI gradually transformed from a dehydrogenase to an oxidase during the long-term storage under room temperature or elevated temperature.

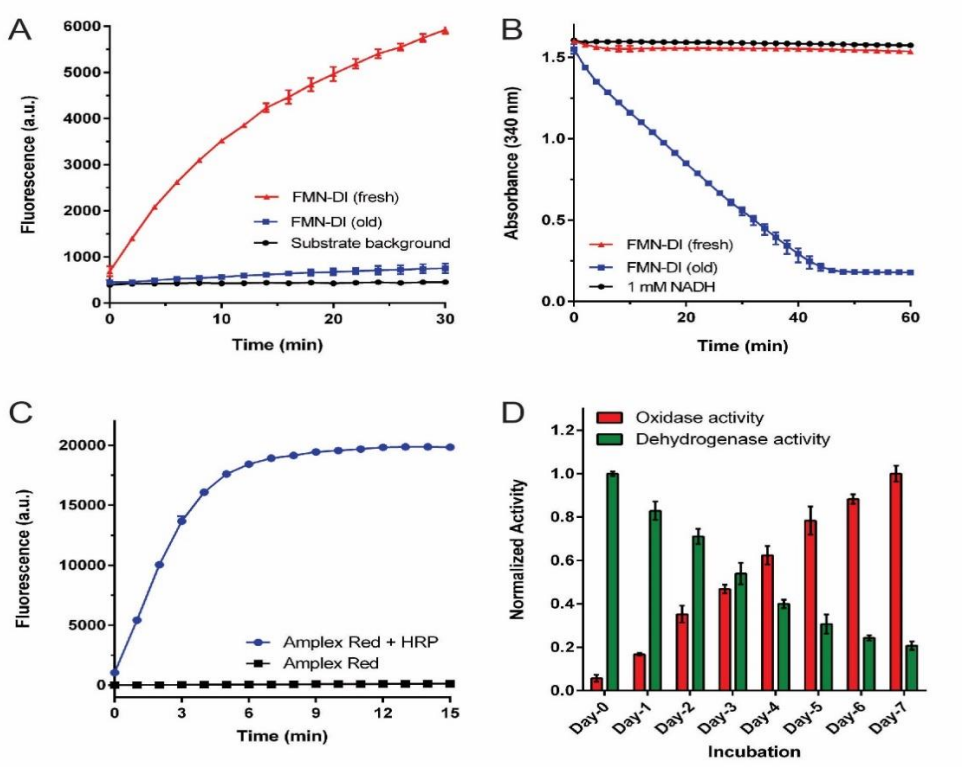

Figure 30. The transformed activities of a FMN-DI during the denaturation. (A) The fresh FMN-DI solution shows a 20-fold higher dehydrogenase activity than a FMN-DI (old) that is stored for more than a year. The dehydrogenase activity is assayed: 1 nM FMN-DI is added into a solution of 500 μM NADH and 500 μM resazurin in pH 7.5, 1 × TBS buffer. (B) An increased oxidase activity for an old FMN-DI solution as compared with a fresh FMN-DI solution. The depletion of NADH is assayed: 1 μM FMN-DI is incubated with 1000 μM NADH, in pH 7.5, 1×TBS buffer. (C) The production of H_2O_2 from the oxidation of NADH is confirmed by the addition of HRP and Amplex Red to produce strongly fluorescent resorufin (excitation ~ 532 nm/ emission ~ 590 nm). Condition: 1 nM HRP and 200 μM Amplex Red are added into the solution of (B) after NADH depletion. (D) The transformed activities of a FMN-DI under the incubation at ~ 25 °C in dark. Error bars generated are the range of 3 replicates.

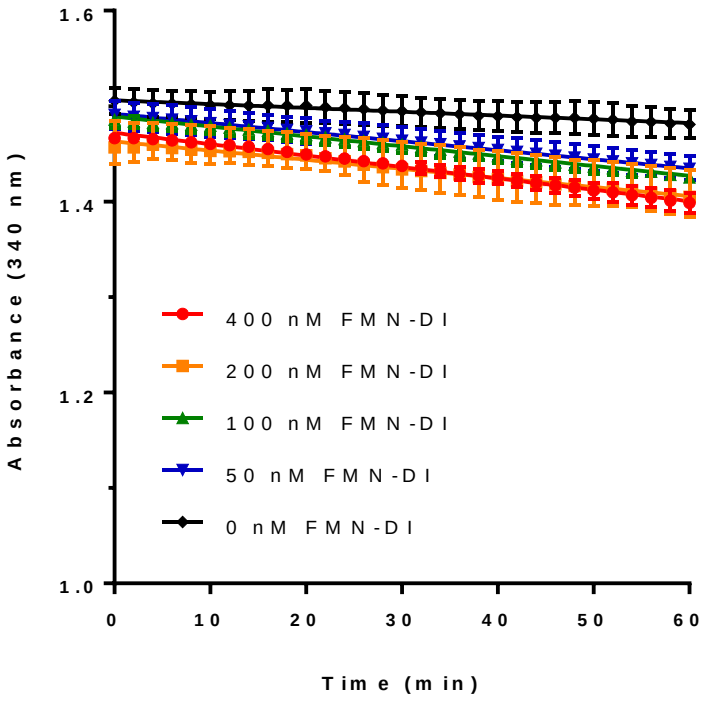

Figure 31. Titration of free FMN-DI solutions for any potential peroxidase activity of catalyzing NADH oxidation by H_2O_2. NADH oxidation is monitored by the decreased absorbance at 340 nm. Conditions: FMN-DI is incubated with 1000 μM NADH and 1000 μM H_2O_2, in pH 7.5, 1×TBS buffer under anaerobic condition.[62] FMN-DI was not observed for obvious NADH peroxidase activity. Error bars generated are the range of 3 replicates.

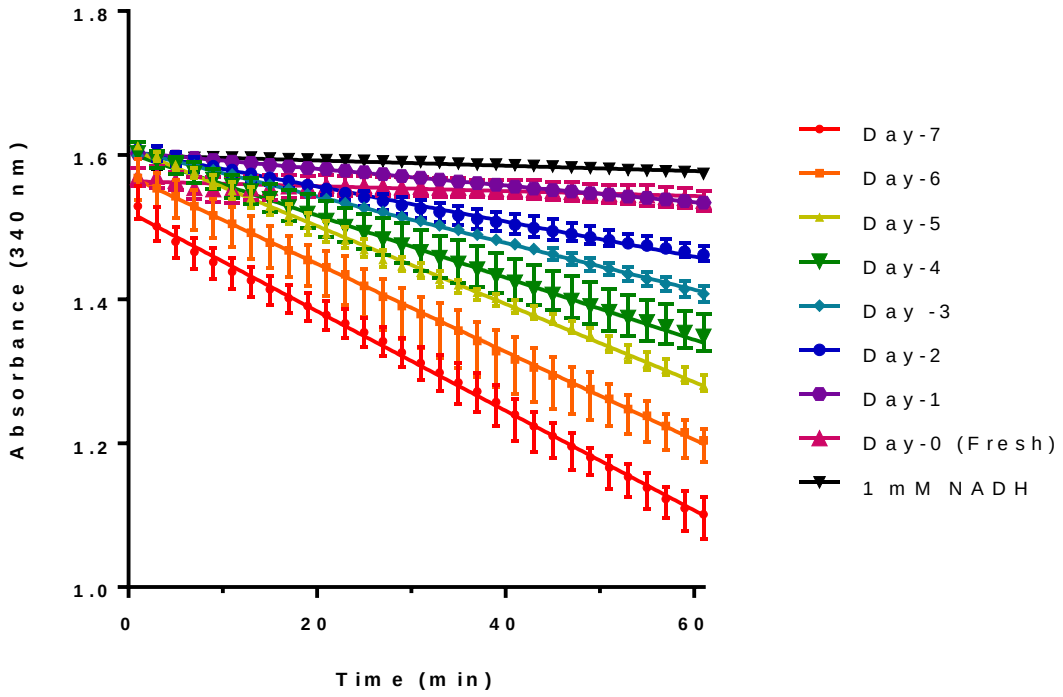

Figure 32. The real-time monitoring of NADH oxidation catalyzed by FMN-DI solutions that were incubated from 0 to 7 days at room temperature. Condition: 1000 μM NADH, 1 μM FMN-DI in pH 7.5, 1×TBS buffer. Error bars generated are the range of 3 replicates.

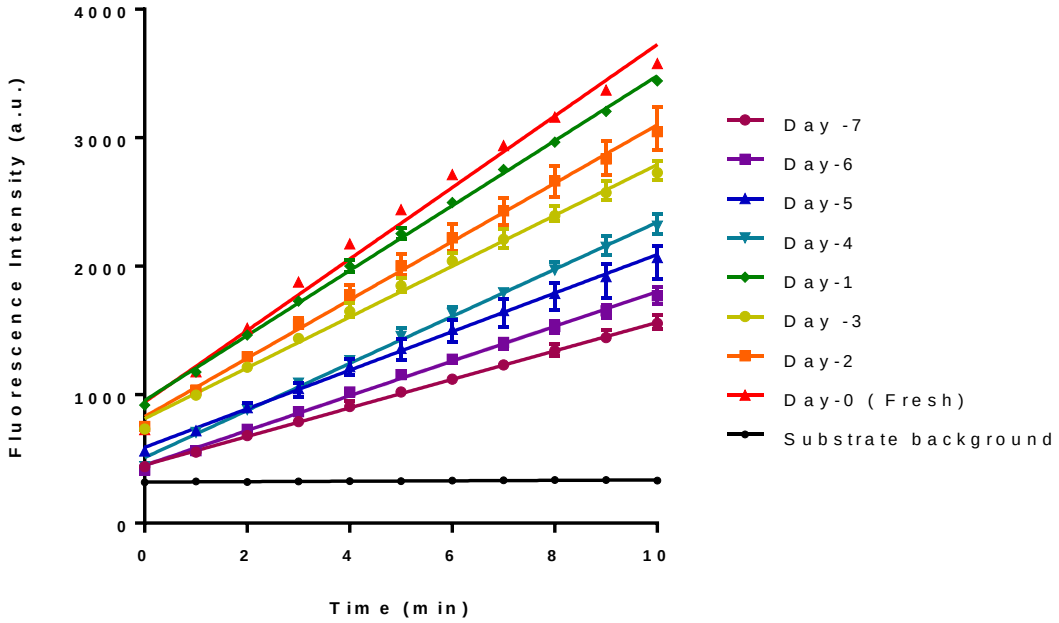

Figure 33. The real-time monitoring of FMN-DI dehydrogenase activities that were incubated from 0 to 7 days at room temperature. Condition: 500 μM NADH, 500 μM resazurin and 1 nM FMN-DI in pH 7.5, 1×TBS buffer. Error bars are the range of 3 replicates.

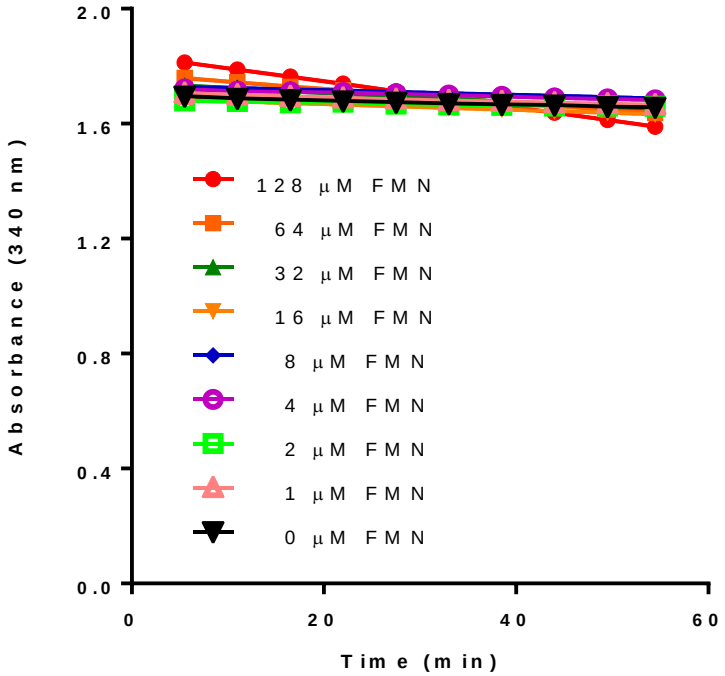

Figure 34. Titration of free FMN solutions for catalyzing NADH oxidation by dissolved oxygen. Only high concentration of free FMN (128 μM) showed obvious higher rate of NADH oxidation than no FMN control. Condition: 1 mM NADH. Error bars are the range of 3 replicates.

3.3.2. Evaluation of FMN binding to DI protein

Different from flavoproteins, such as succinate dehydrogenase,[75] FMN was not covalently linked to DI, but tightly-bound to the protein. Therefore, we hypothesized that the binding strength between the FMN cofactor and DI protein might influence the observed functional change of the enzyme. The tightly-bound FMN was suggested to be critical for the dehydrogenase activity, and was also less accessible to oxygen molecules that showed more resistance to the aerobic oxidation in aqueous solution (low oxidase

activity). Conversely, the binding between FMN and the DI protein was gradually destabilized during the long-term storage under room temperature. The loosely-bound FMN in DI resulted in the loss of the dehydrogenase activity. However, this dissociated FMN could work as an electron mediator between DI and dissolved molecular oxygen, and the DI exhibited more NADH oxidase activity. To test this hypothesis, a molecular weight cut-off filter (3 kD) was first used to wash the solutions of fresh FMN-DI and aged FMN-DI. If FMN is tightly bound with DI, most of the FMN molecules will still stay with protein on the top of the filter. If FMN is dissociated from the DI protein, free FMN molecules will pass through the filter membrane. As shown in **Table 1**, the relative ratio of FMN to DI was characterized using their unique absorbance at 452 nm (FMN) and 280 nm (DI protein). For a fresh FMN-DI solution, the value of $A_{452\ nm}/A_{280\ nm}$ was similar (~ 0.12 – 0.13) even after two washes, indicating that FMN was tightly bound with DI protein. Conversely, for an aged FMN-DI solution (one year old), the value of $A_{452\ nm}/A_{280\ nm}$ decreased from 0.144 to 0.072 after one wash, and was further decreased to 0.048 after two washes. This suggested that FMN was dissociated from DI when DI was stored for a long period.

The FMN-DI solution produced from a thermophilic bacterium contains ~ 0.5 FMN molecule per monomeric protein. When used for various applications, excess FMN molecules are added into the DI solution to saturate the binding of FMN to protein.[50] Thus, an attempt was made to add more free FMN molecules into the DI solution for enhancing dehydrogenase and oxidase activities. As shown in **Figure 35A**, the dehydrogenase activity of a fresh FMN-DI solution was increased as adding more FMN from 0 to 16 nM, and was almost saturated for FMN > 16 nM. In a control experiment,

free FMN by itself did not catalyze the hydride transfer between NADH and resazurin (**Figure 36**). Since FMN-DI has a smaller K_m of ~ 20- 40 μM for NADH,[62] under the high NADH concentration of 1 mM, an assumption was made that the reaction rate (initial velocity, *V*) is directly correlated to the concentration of the 'FMN-$DI_{(DH)}$ complex' (FMN-$DI_{(DH)}$ catalyzes the dehydrogenation reaction), where $V \sim k*[FMN\text{-}DI]$ and $k \sim k_{cat}$. By fitting the dehydrogenase activities with the addition of free FMN molecules, the binding strength of FMN to the DI protein was able to be estimated**.** As shown in **Figure 35B,** the apparent dissociation constant ($K_{d,\,app}$) of FMN with DI protein was ~ 0.47 nM, which supported the hypothesis that the tightly bound FMN-DI contributed to the dehydrogenase activity. Similarly, a titration with the addition of free FMN into a fresh DI solution for enhancing oxidase activity was also performed. As shown in **Figure 35C**, the NADH oxidation by FMN-DI protein was increased with the addition of excess FMN from 0 to 128 μM. In a control experiment, free FMN by itself only showed weak oxidase activity at high micro-molar concentrations (**Figure 34**). As described above, the oxidase activity was directly correlated to the concentration of 'FMN-$DI_{(O2)}$ complex' (FMN-$DI_{(O2)}$ has stronger NADH oxidase activity). In **Figure 35D**, the apparent dissociation constant of FMN binding to the DI protein for FMN-$DI_{(O2)}$ was $K_{d,app}$ ~ 82 μM, by fitting the oxidase activities with the addition of free FMN molecules. Obviously, the apparent K_d value of FMN-$DI_{(O2)}$ for oxidase activity was much larger than that of FMN-$DI_{(DH)}$ for dehydrogenase activity. This result further supported our hypothesis that the tight FMN-DI interaction contributed to the strong dehydrogenase activity and the weak FMN-DI interaction was responsible for the increased oxidase activity.

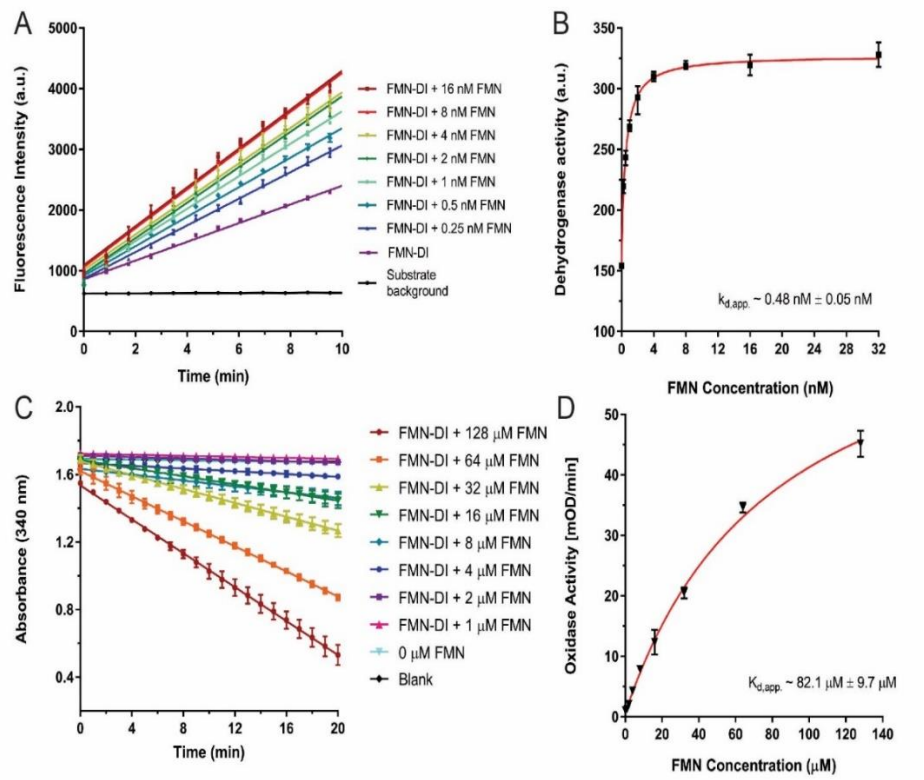

Figure 35. The titration of free FMN molecules for affecting the activities of a fresh FMN-DI solution. (A) Titration of excess FMN molecules into a FMN-DI solution for enhancing the dehydrogenase activity: 0.5 nM FMN-DI is incubated with 0 – 16 nM free FMN, and is assayed by adding 500 μM NADH and 500 μM resazurin in pH 7.5, 1×TBS buffer. (B) The initial velocities of reactions are fitted with the addition of free FMN molecules for estimating the apparent dissociation constant of FMN binding to DI for dehydrogenase activity. (C) Titration of excess FMN molecules into a FMN-DI solution for enhancing the oxidase activity: 200 nM FMN-DI is incubated with 0 – 128 μM free FMN, and is assayed by adding 1000 μM NADH in pH 7.5, 1×TBS buffer. (D) The initial velocities of reactions are fitted with the addition of free FMN molecules for estimating the apparent dissociation constant of FMN binding to DI for oxidase activity. Error bars are the range of 3 replicates.

Wash Steps	Fresh FMN-DI			Old FMN-DI		
	A280	A452	A452/ A280	A280	A452	A452/ A280
Prior to wash	8.67	1.11	0.13	8.22	1.13	0.14
1	7.99	0.96	0.12	7.41	0.53	0.072
2	7.71	0.93	0.12	6.62	0.32	0.048

Table 1. Removal of FMN from DI protein by molecular-weight cutoff filtration.

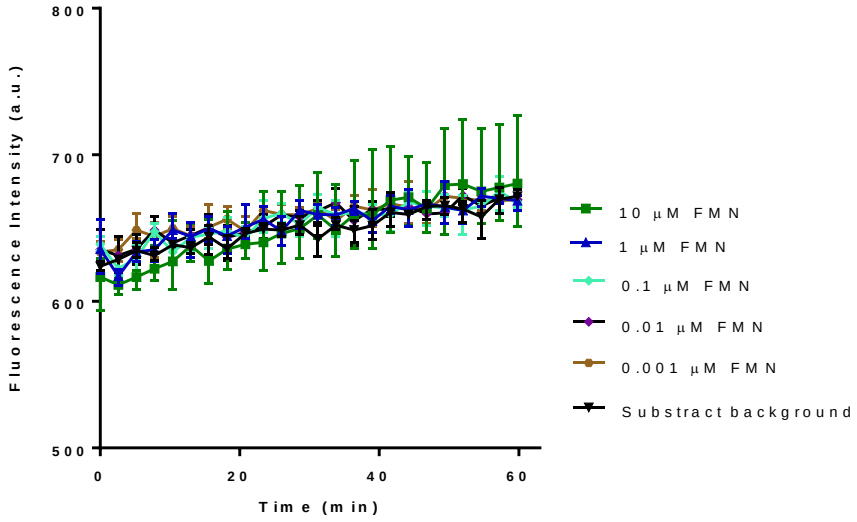

Figure 36. Titration of free FMN solutions for dehydrogenase activity that converts resazurin to resorufin by NADH. Condition: 500 µM NADH and 500 µM resazurin in pH 7.5, 1×TBS buffer. Error bars are the range of 3 replicates.

3.3.3. CD Measurement of Protein Folding

Circular dichroism (CD) was used to analyze the folding state of FMN-DI. As shown in **Figure 37A**, both the fresh FMN-DI and the old FMN-DI solutions showed negative CD signals at 210 -222 nm, which suggested alpha helical structures.[76] The old FMN-DI solution showed a shifted positive peak at ~198 nm as compared with the positive peak at ~ 193 nm for the fresh FMN-DI solution. This shifted absorbance might suggest an increased beta-sheet structure for the old FMN-DI solution. In **Figure 37B**, the binding of FMN to DI was also analyzed by CD,[77] where the fresh FMN-DI solution showed a positive CD signal at ~ 450 nm with the indication of protein-bound FMN. The old FMN-DI solution showed a relatively weaker CD signal, suggesting the destabilized FMN-DI binding. As a control, the free FMN solution did not show an obvious CD signal at ~ 450 nm.

Consistent with the observations in this work, other flavoproteins have been discovered to be either strong dehydrogenases (oxygen resistant) or strong oxidases (accept oxygen), for example, FAD-glucose oxidase[78] and FAD-glucose dehydrogenase.[79] It was suggested that the binding of FAD to the protein was responsible for the different activities between FAD-glucose oxidase and FAD-glucose dehydrogenase. Glucose oxidase has a surface-bound FAD that facilitates the electron transfer from $FADH_2$ to molecular oxygen, while glucose dehydrogenase has a more deeply bound FAD with little access to oxygen.[80] Glucose oxidase can be further modified into a glucose dehydrogenase by mutating the amino acids associated with binding to FAD, which shield it from oxygen.[80]

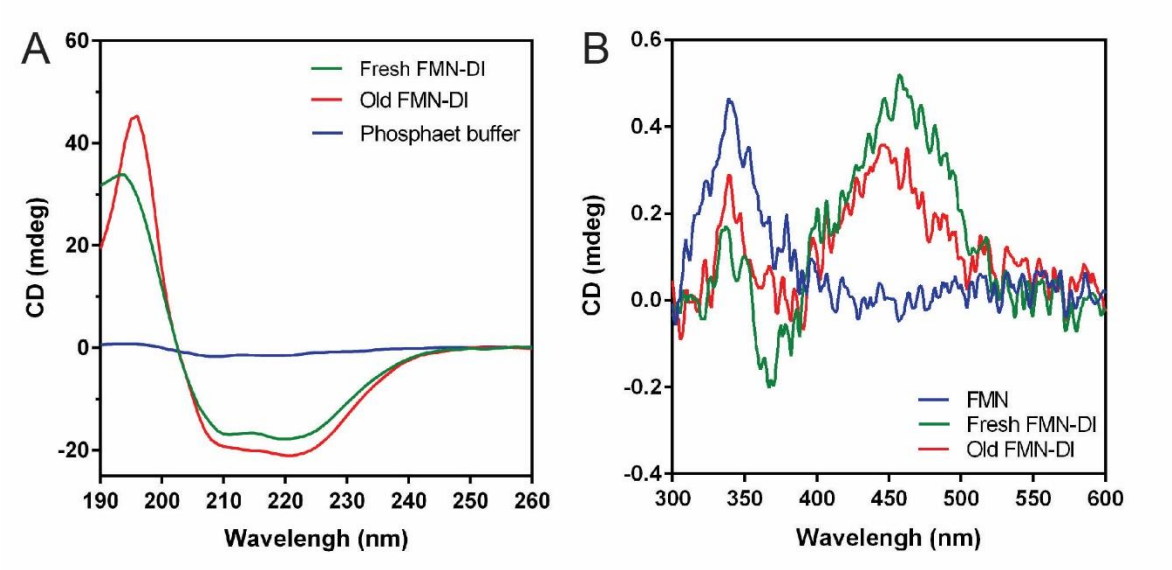

Figure 37. CD spectrum of FMN-DI complexes. (A) CD spectrum of DI proteins from 190 – 260 nm. Condition: 10 μM DI in pH 7.5, 20 mM sodium phosphate buffer. (B) CD spectrum (300 – 600 nm) for 100 μM solutions of free FMN (blue), fresh FMN-DI (green) and old FMN-DI (red).

3.4. Conclusion

In summary, FMN-DI was observed to undergo a functional transformation from a primary dehydrogenase to a primary oxidase during the protein storage and denaturation process. The transformed activities were induced by the alteration of the binding strength between the FMN cofactor and the DI protein. For a fresh FMN-DI solution, FMN was tightly bound to the protein and showed a strong dehydrogenase activity and resistance to oxygen. As FMN started to dissociate from the protein during denaturation, the dehydrogenase activity was gradually reduced. Meanwhile, the enzyme exhibited increased oxidase activity as more FMN became weakly bound to DI. The observed functional transformation may also apply to other FMN or FAD-bound

enzymes that are widely used in biological redox reactions. These studies not only enhance our understanding of functional transformations during protein denaturation, but may also provide practical insights into flavoprotein-based sensing and biocatalysis (e.g. side product and peroxide generation due to the denature-induced activity transition of enzymes).[50, 62]

3.5. Acknowledgements

The following authors contributed to this work: Scott Huston, John Collins, Fangfang Sun, Ting Zhang, Timothy D. Vaden, Y. –H. Percival Zhangc, and Jinglin Fu. This work is supported by an Army Research Office YIP award (W911NF-14-1-0434), the Cottrell College Science Award to J.F. and the start-up fund to J.F. from Rutgers University-Camden. J.C. was sponsored by the summer undergraduate research of the Cottrell College Science Award. S.H. was a summer fellow sponsored by the AEOP URAP program. Authors are also grateful to the Equipment Leasing Funds from the State of New Jersey.

Chapter 4

DNA-Crowded Enzyme Nanoparticles with Enhanced Activities and Stabilities

Abstract

Nucleic acids have emerged as a remarkable nanoscale building material due to their well-defined structural properties and ease of functionalization. Recently, DNA nanostructures have been shown to immobilize enzymes and regulate their activities. An interesting observation of enzymes immobilized onto DNA scaffolds is that they tend to show enhanced catalytic activity and stability compared to free enzymes in solution. In this work, enzyme-DNA nanoparticles are created using the hybridization chain reaction to grow DNA from the surface of two enzymes: horseradish peroxidase (HRP) and glucose-6-phosphate dehydrogenase (G6PDH). The local molecular crowding effect, caused by the DNA creates a microenvironment around the enzymes, is shown to enhance their activities and stabilities.

4.1. Introduction

Enzymes play critical roles in cellular metabolism for catalyzing complex synthetic pathways to convert chemicals and derive energy which is vital to life. Biology has evolved various ways to maintain the functional stability and proper folding of enzymes under stressed conditions, employing molecular chaperones,[81] polyanionic phosphate[41] and small-molecule osmolytes (e.g. trimethylamine N-oxide).[67] The ability to control enzyme activity and stability is important for a variety of noncellular enzyme applications, ranging from diagnostics and drug delivery to the synthesis of high-value chemicals and bioenergy conversion.[82] Recently, nucleic acids nanostructures have emerged as scaffolds to immobilize enzymes and regulate their activities on the nanoscale.[34a, 83] For example, enzyme cascades were organized on DNA nanostructures with controlled spacing distance between them to facilitate the transport of intermediate molecules.[2] The cofactor-modified DNA was used as a biomimetic "swinging arm" to transfer hydrides between two dehydrogenases.[37] A nanomechanical switch made from a DNA nanostructure was used to modulate enzymes activities by regulating the distance between enzymes or enzyme/cofactor pairs, as well as by directionally shifting cofactor swinging arms.[84] More interestingly, enzymes immobilized on nucleic acids nanostructures are found to be more active and stable than free, non-immobilized enzymes. Such examples include enzyme conjugation to giant λDNA,[85] enzyme assembly on 2D DNA origami[39] and DNA nanocaged enzymes,[86] as well as enzyme attachment to a DNA scaffold with affinity to substrate molecules.[87] These observations have suggested a widespread beneficial effect of enzyme-DNA nanostructure interactions. However, a typical DNA origami nanostructure contains nearly 200 unique oligonucleotides with

complex preparation procedures and low achievable concentrations of a few nanomolar (nM). This low-production scale of DNA nanostructures is several orders of magnitude lower than standard enzyme production. Here, a simple and robust approach is described for constructing DNA-crowded enzyme nanoparticles by directly growing long double-stranded DNA on the enzyme surface. The DNA-crowded enzyme nanoparticles showed increased activities and stabilities against various storage conditions.

4.2. Materials and Methods

4.2.1. Materials

Sodium phosphate dibasic, sodium chloride, tris base, magnesium chloride, 10x Tris-buffered saline (TBS), and DNA grade water were all purchased from Fisher Scientific (Waltham, MA.). Horseradish peroxidase (HRP), glucose oxidase (GOx), hexokinase (HEK, rabbit muscle), β-Nicotinamide adenine dinucleotide (NAD^+), glucose-6-phosphate (G6P), glucose, and 2,2'-Azino-bis(3-ethylbenzothiazoline-6-sulfonic acid) diammonium salt (ABTS) were all purchased from Sigma Aldrich (St. Louis, MO.). Glucose-6-phosphate dehydrogenase was purchased from Worthington Biochemical Company (Lakewood, NJ). All oligonucleotides were purchased from Integrated DNA Technologies. Initiator strand (I): 5'- AGT CTA GGA TTC GGC GTG GGT TAA AAA AAA AAA A-amine -3'; hairpin 1 (HP-1): 5'- TTA ACC CAC GCC GAA TCC TAG ACT CAA AGT AGT CTA GGA TTC GGC GTG -3'; hairpin 2 (HP-2): 5'- AGT CTA GGA TTC GGC GTG GGT TAA CAC GCC GAA TCC TAG ACT ACT TTG -3'

4.2.2. SPSC Buffer Solution Preparation

The buffer was prepared as previously reported in literature.[88] A 1 × sodium phosphate sodium chloride (SPSC) containes 50 mM sodium phosphate and 500 mM sodium chloride. The pH of the buffer solution is adjusted to 7 using 1 M hydrochloric acid (HCl).

4.2.3. Assembly of DNA-Crowded Enzyme Nanoparticles

DNA-crowded enzyme nanoparticles were prepared by first snap cooling hairpins 1 and 2 separately in 1x SPSC (pH 7.0), at 3x their final concentration, by heating to 95 °C for 5 minutes, followed by cooling at 23 °C for 30 minutes. 300 nM enzyme-I solution was prepared (3x final concentration) in 1x SPSC (pH 7.0), followed by the addition of H1 and H2 strands to a final concentration of 100 nM enzyme. The solution mixture was then incubated in the dark for at least 3 hours on a rocker (Model, manufacture) at 50 rpm, Note: Control solutions were incubated similarly in 1x SPSC without the addition of hairpin strands

4.2.4. Bulk Solution Enzyme Assays

A 96-well plate reader (Cytation 3, Biotek) was used to monitor enzyme activity through absorbance changes of the samples. The enzyme samples and substrates were loaded in the wells of the 96-well half area plate with a final concentration of DNA-crowded enzymes of ~ 1 nM in 1× TBS (Tris buffered saline with 1 mM $MgCl_2$, pH 7.5) at a volume of 70 μL for most assays. Enzyme solutions were allowed to incubate at 2x the final assay concentration for 20 minutes at room temperature prior to the addition of substrate. For a typical HRP assay, H_2O_2 and ABTS were used as substrates and the

enzyme activity was measured by monitoring the increase in absorbance at 420 nm due to the oxidation of ABTS to $ABTS^{\bullet+}$. For a typical G6PDH assay, G6P and NAD^+ were used as substrates, and the enzyme activity was measured by monitoring the increased absorbance at 340 nm due to the reduction of NAD^+ to NADH. Activities of enzyme solutions were determined by the initial linear velocity. V_{max} and *Km* values were determined by fitting *velocity vs. substrate concentration* with Michaelis-Menten equation, using GraphPad Prism 6. Calibration curves were used to convert V_{max} to k_{cat}.

4.2.5. Long Term Stability of DNA-Crowded Enzyme Nanoparticles

To measure the long term stability of DNA-crowded enzyme nanoparticles, 100 nM enzyme samples, in 1x SPSC (pH 7.0), were stored at room temperature for a period of 10 weeks. Once a week, an aliquot of the samples was taken, and then used to measure the activity of the sample using the typical activity measurement procedure (see section 4.2.4).

4.2.6. Freeze-Thaw Stability of DNA-Crowded Enzyme Nanoparticles

To measure the stability of DNA-crowded enzyme nanoparticles with repeated freezing and thawing, a 20 μL aliquot of each sample was taken and set aside for this experiment after it had been prepared. After measuring the activity of each sample to determine a baseline, each sample was placed into the – 80 °C freezer for 30 minutes to freeze. Once the samples were frozen, they were taken out of the freezer and allowed to thaw at room temperature for 10-20 minutes. Once thawed, an aliquot was taken from each sample and used to measure the activity (see section 4.2.4 for activity

measurement). Samples would then be placed back into the freezer for another 30 minute freeze, and the process was repeated for each freeze-thaw cycle.

4.2.7. Thermal Stability of DNA-Crowded Enzyme Nanoparticles

To measure the thermal stability of DNA-crowded enzyme nanoparticles, enzyme samples were diluted to 10 nM with 1x TBS-Mg (pH ~7.4). Samples were then incubated in the thermocycler at a set temperature for 1 hour, while an internal control concurrently was incubated at room temperature. Once the incubation was complete, the activity of each sample was determined using the activity measurement procedure for DNA crowded enzymes described above (see section 4.2.4).

4.2.8. pH Activity of DNA-Crowded Enzyme Nanoparticles

To measure the pH activity of DNA-crowded enzyme nanoparticles, enzyme samples were incubated at two times the assay concentration in a universal buffer solution (20 mM glycine, 20 mM sodium citrate, 20 mM magnesium acetate, 20 mM tris base) at various pH values for 20 minutes, and then assayed in the same buffer using a procedure very similar to that described in section 4.2.4.

4.2.9. Enzyme Binding to Centrifuge Tube Control

To determine whether the activity enhancements that were observed were real, and not due to DNA preventing the enzyme from binding to the sides of the centrifuge tubes during our experiments, Cy3 labeled HRP was used to measure the change in fluorescence during the course of the experiment. A decrease in fluorescence would indicate a loss of enzyme due to binding to the centrifuge tube, a constant fluorescence means that no enzyme is binding to the tube. This control was run for each stability test

that was performed. To do so, each experiment would be repeated as close to the actual experiment as done previously, but with the Cy3-labeled HRP. After treatment, the sample would be diluted to 10 nM HRP-Cy3, and allowed to incubate for 20 minutes at room temperature. Then, the fluorescence of the samples would be measured using the fluorescence polarization function of the Cytation 3 plate reader, using the Cy3 FP filter and the gain set to 70. The well volume for each sample was 100 µL. Total fluorescence of each sample was then determined by summing the parallel and perpendicular fluorescence values.

4.2.10. Atomic Force Microscopy

2 µL 100 nM sample solution was first deposited onto a freshly cleaved mica surface (Ted Pella, Inc.) and left to adsorb for 2 minutes. 80 µL of 1 x TAE-Mg2+ buffer was added to the sample and 2 µL 100 mM Ni2+ was added to enhance the adsorption of the DNA-crowded enzyme nanoparticles on the mica. An extra 40 µL of 1 x TAE-Mg^{2+} buffer was deposited to the mica. The samples were scanned with SCANASYST-Air probe (Bruker, Inc.) using “Scanasyst in air mode” of a Multimode 8 AFM (Bruker Corporation).

4.2.11. Electrophoresis

Native PAGE characterization of DNA structures: Native PAGE gels (3%) were prepared at room temperature and run for 2.5h at a constant voltage of 200V and subsequently stained with SYBR Green and visualized with a Molecular Imager Gel Doc XR+ System (Bio-Rad).

4.2.12. Purification of Oligonucleotides

Oligonucleotides purchased from Integrated DNA Technologies (IDT) were purified by denaturing PAGE. Denaturing PAGE gels (8-10%) were prepared at room temperature.

4.2.13. Bioconjugation, Separation and Dye Labelling

Enzymes were conjugated to the initiator strand by first reacting 3'-amine modified initiator with SPDP for 2 hours on a rocker (50 rpm) at room temperature in 50 mM HEPES buffer (pH 8.5). Excess SPDP was removed by washing SPDP-initiator with a 10kD amicon MWCO filter 3 times with DNA grade water. The following day, enzyme was first reacted with SPDP by incubating for 1 hour at room temperature, on the rocker (50 rpm) in 50 mM HEPES buffer (pH 8.5). SPDP-modified enzyme was then washed 3 times with 50 mM HEPES (pH 7.5) using an amicon filter (30 kD cutoff). Then, enzyme-SPDP would be mixed with an 8-10 fold excess initiator-SPDP, and incubated on the rocker (50 rpm) for 1 hour, at room temperature, in 50 mM HEPES buffer (pH 7.5). Enzyme-initiator conjugates were then washed again, 3x times, with 50 mM HEPES (pH 7.5). Enzyme-initiator conjugates were purified using anion exchange FPLC.

4.2.14. Particle Size Measurement of DNA-Crowded Enzyme Nanoparticles

Particle size measurements of DNA-crowded enzyme nanoparticles were performed using a Zetasizer (Malvern) to measure the dynamic light scattering of 100 nM enzyme-initiator, with varying amounts of hairpins, in filtered 1x SPSC buffer (pH 7.0).

4.3. Results and Discussion

4.3.1. Structural Characterization of DNA-Crowded Enzyme Nanoparticles

As shown in **Figure 38A**, the construction of DNA-crowded enzyme nanoparticles involves two steps: (1) the conjugation of an initiator strand to an enzyme and (2) the growth of double-helix (ds) DNA on the enzyme surface by the initiator-triggered hybridization chain reaction (HCR).[88] One initiator on the enzyme surface can trigger the hybridization of a long DNA duplex with alternative hybridization of hairpin 1 and 2. The size of the DNA duplex can be controlled by the initiator-to-hairpin ratio. The long HCR duplex on the enzyme surface behaves as a flexible 'DNA hair' (non-nick dsDNA's persistence length is ~ 50 nm, while the HCR duplex has many nick points that make it easier to bend) to wrap around the enzyme. In this way, the enzyme is surrounded by a local DNA duplex with high density. As shown in **Figure 38B**, gel electrophoresis was used to characterize the growth of the long DNA duplex on the enzyme surface, where large DNA duplexes with slower mobility were observed with the addition of more hairpin substrates. The fluorescent imaging of Cy3-labelled enzyme showed that the enzyme migrated together with the large DNA duplex. Dynamic light scattering (**Figure 38C)** was using to measure the stepwise growth of the DNA-crowded enzyme nanoparticles as the amount of added hairpins is increased from 1-16x to that of the enzyme. The inset of **Figure 38C** is an atomic force microscope image depicting the growth of DNA "hairs" from the enzymes surface.

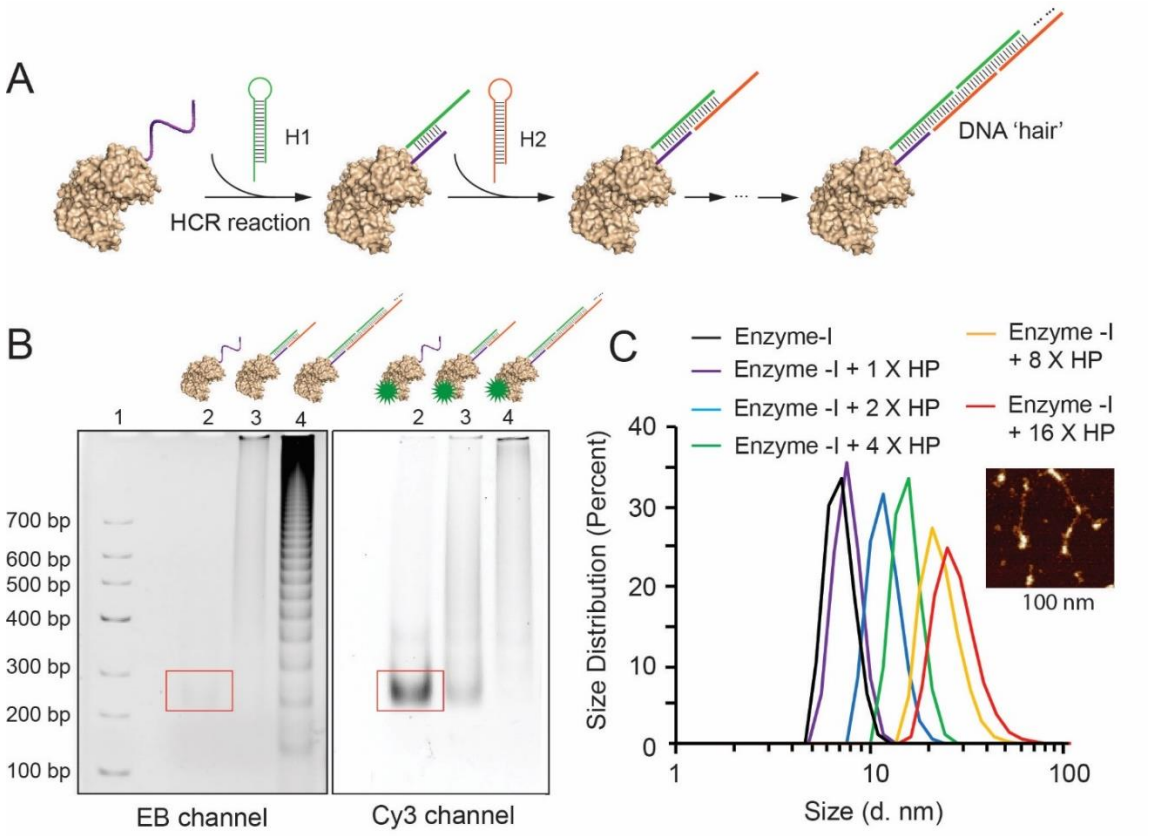

Figure 38. The concept of DNA-crowded enzyme nanoparticles. (A) The construction of a long DNA duplex on an enzyme surface by HCR. (B) (3%) PAGE characterization of DNA-crowded enzymes with EB staining (left) of DNA and fluorescent imaging (right) of Cy3-labelled G6PDH. Lane 1: DNA ladder; Lane 2: 1 μM initiator-conjugated G6PDH (G6PDH-I); Lane 3: 1 μM G6PDH-I + hairpins (1×); Lane 4: 1 μM G6PDH-I + hairpins (10×). (C) DLS analysis of DNA-crowded enzyme nanoparticles with the titration of hairpins. Inset: AFM image of DNA-crowded enzyme nanoparticles.

4.3.2. Activity Characterization DNA-Crowded Enzymes Nanoparticles

Next, the enzyme activities depending on the growth of long DNA duplex on the enzyme surface was evaluated. As shown in **Figure 39A**, the G6PDH-initiator (G6PDH-I) conjugate was incubated with excess hairpins from 1 to 128-fold. More than 200% activity enhancement was observed when the enzyme was incubated with 16-fold or more excess hairpins. As a control, non-initiator conjugated enzymes were also incubated with these hairpins, but these enzymes only showed slight increase (< 20%) of enzyme activities with the addition of excess hairpins. Similar results were also observed for the HRP-initiator (HRP-I) conjugate where the enzyme showed more than 300% enhanced activity by adding more than 32-fold HPs (**Figure 39B**). To evaluate the effect of labelled numbers for initiator strands, HRP was conjugated to 1, 2 and 3 initiators. Activities of HRP were affected little by conjugating to DNA strands (**Figure 40A**). As shown in **Figure 39C**, HRP-I_2/HCR and HRP-I_3/HCR complexes showed higher activity than the HRP-I_1/HCR complex, possibly due to the fact that more conjugated initiators would produce higher dsDNA density on the protein surface by HCR. However, some enzymes may show seriously reduced activities as conjugating more DNA molecules (> 3) on the enzyme surface (e.g. G6PDH-I_x in **Figure 40B**).[34a] To avoid the damaged activities, conjugating an enzyme with no more than two initiator strands for assembling HCR structures on the enzyme surface is recommended.

To gain more mechanistic insight into the enhanced enzyme activities, the Michaelis-Menten kinetics of enzyme-HCR complexes for HRP and G6PDH were evaluated (**Figure 41)**. As shown in **Table 2**, HRP-I_1/HCR, HRP-I_2/HCR and HRP-I_3/HCR complexes all showed increased turnover numbers as compared to non-HCR

enzymes HRP-I_1, HRP-I_2, and HRP-I_3, suggesting an inherently higher catalytic activity of the enzymes. HRP-I_2/HCR and HRP-I_3/HCR showed ~ 2.7-hold enhancement of k_{cat} values, whereas HRP-I_1/HCR showed less enhancement, at ~ 1.6-hold. This difference of enhanced turnover numbers is consistent with our observation that enzymes labelled with more initiator strands produced more enhanced activity, as seen in **Figure 39C**. Similarly, G6PDH-I_x/HCR complexes also showed higher turnover numbers (~ 2 -3 fold) than non-HCR enzymes of G6PDH-I_x. However, G6PDH-I_3/HCR ($k_{cat, NAD}$~ 210 s^{-1}) was significantly less active than G6PDH-I_1/HCR ($k_{cat, NAD}$~ 327 s^{-1}) and G6PDH-I_2/HCR ($k_{cat, NAD}$~ 378 s^{-1}), which was resulted from the low activity of G6PDH-I_3. In contrast, detailed kinetic analyses showed that the K_m (the Michaelis-Menten constant) varied little between enzyme-HCR and free enzyme-initiator for most substrates, suggesting that the HCR duplex does not substantially hinder diffusion of small-molecule substrates to the enzymes active site.

The activity enhancement for DNA-crowded enzyme nanoparticles is consistent with recent reports of nanocaged enzymes,[86a] enzyme attachment to nucleic acid nanostructures of (λDNA)[38] and a 2D rectangular DNA origami[39], or a DNA scaffold that bound to enzyme substrates.[87] It has been observed as a widespread effect of enzyme-DNA nanostructure interactions. A recent study suggested that the negatively charged DNA nanostructures might create a local pH near the DNAs surface that is lower than that of the bulk solution. The activity of the enzyme attached on DNA nanostructures was promoted due to the optimal pH environment of the anchored enzymes, e.g. acidic active HRP.[89] To test this, the DNA-crowded enzyme nanoparticles were incubated in buffer solutions with the pH ranging from 4 to 10, followed by evaluating the enzyme activities.

As shown in **Figure 42**, the normalized activities of DNA-crowded enzyme nanoparticles showed a similar pH trend as compared to free enzymes without DNA crowding. In addition, G6PDH is most active at a basic pH. The increased acidity near the DNA surface cannot be used to explain the promoted activities of G6PDH-HCR complexes at neutral pH. These result indicated that the DNA scaffolds contributed little to the pH activities of enzyme-HCR complexes. Other mechanisms may be proposed to explain the enhanced activities, such as micro-environment crowding induced by giant and ordered DNA molecules, the substrates affinity to DNA scaffolds, and the stabilized hydration layer of hydrogen-bounded water molecules near the DNA backbone phosphates.[90] Multiple studies[66] have described that proteins are more stable and active in a highly ordered, hydrogen-bonded water environment, possibly due to stabilization of the hydrophobic interactions of a folded protein through an increase in the solvent entropy penalty upon unfolding. Consistent with this model, polyphosphate has been shown to act as a generic chaperone stabilizing a variety of enzymes.[41]

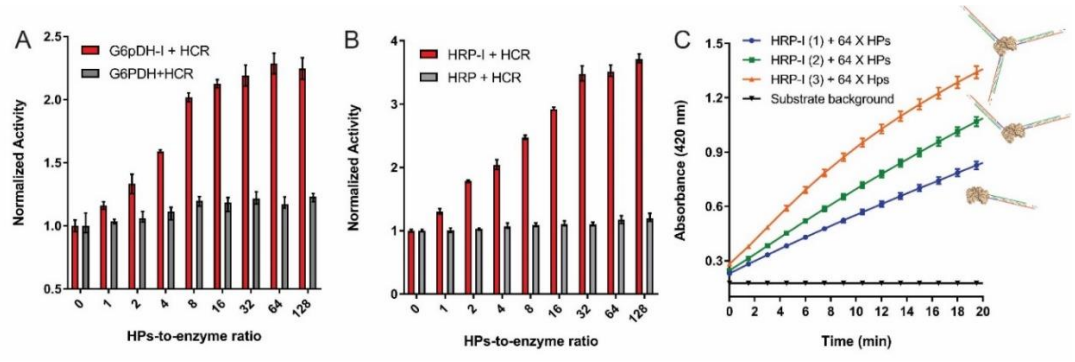

Figure 39. Evaluation of DNA-crowded enzyme complexes. (A) Titration of HPs-to-enzyme ratio for affecting DNA-crowded G6PDH activity; (B) Titration of HPs-to-enzyme ratio for affecting DNA-crowded HRP activity. (C) Titration of labelled initiators per enzyme for affecting DNA-crowded HRP activity. Error bars represent the range of 3 replicates.

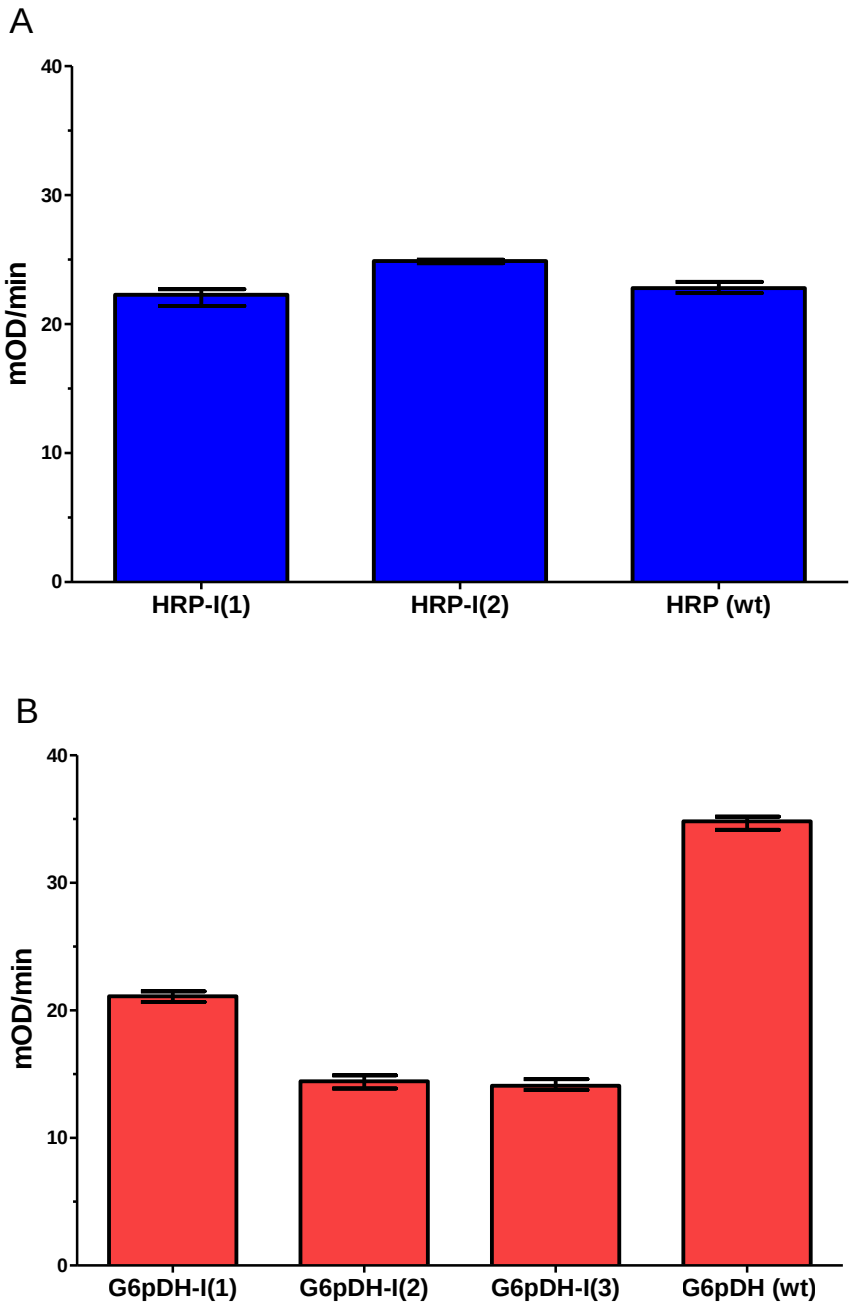

Figure 40: Activities of enzymes after conjugation to the initiator strand. (A) HRP-Initiator and (B) G6PDH-Initiator. Error bars represent the range of three replicates.

A

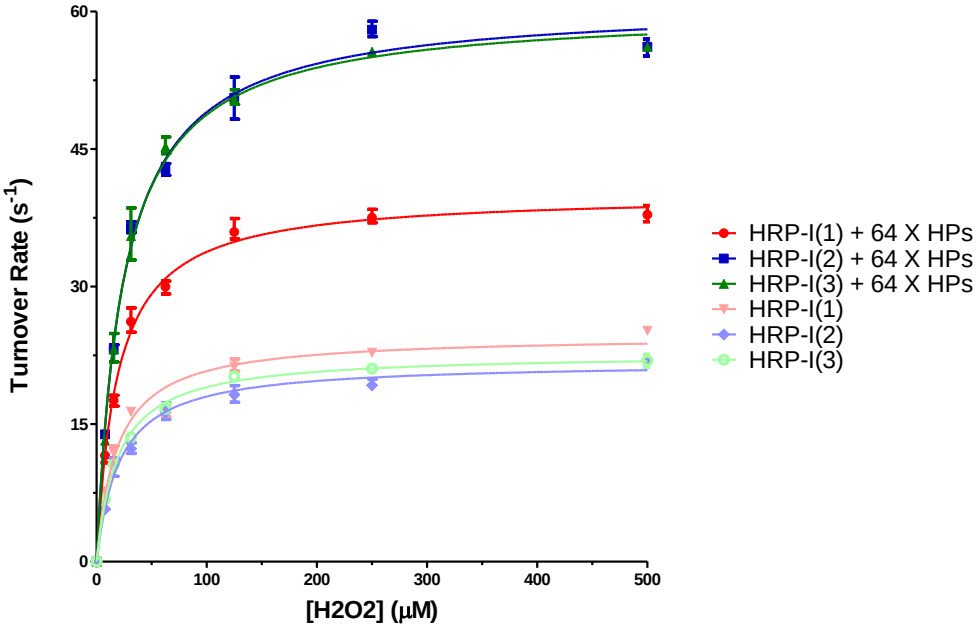
Turnover Rate (s^{-1})
[H2O2] (μM)
HRP-I(1) + 64 X HPs
HRP-I(2) + 64 X HPs
HRP-I(3) + 64 X HPs
HRP-I(1)
HRP-I(2)
HRP-I(3)

B

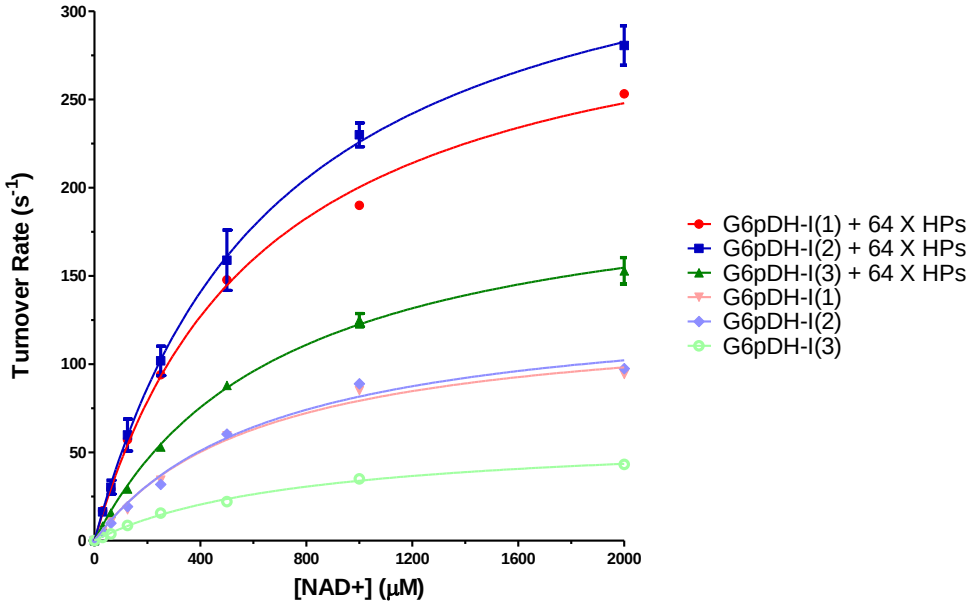
Turnover Rate (s^{-1})
[NAD+] (μM)
G6pDH-I(1) + 64 X HPs
G6pDH-I(2) + 64 X HPs
G6pDH-I(3) + 64 X HPs
G6pDH-I(1)
G6pDH-I(2)
G6pDH-I(3)

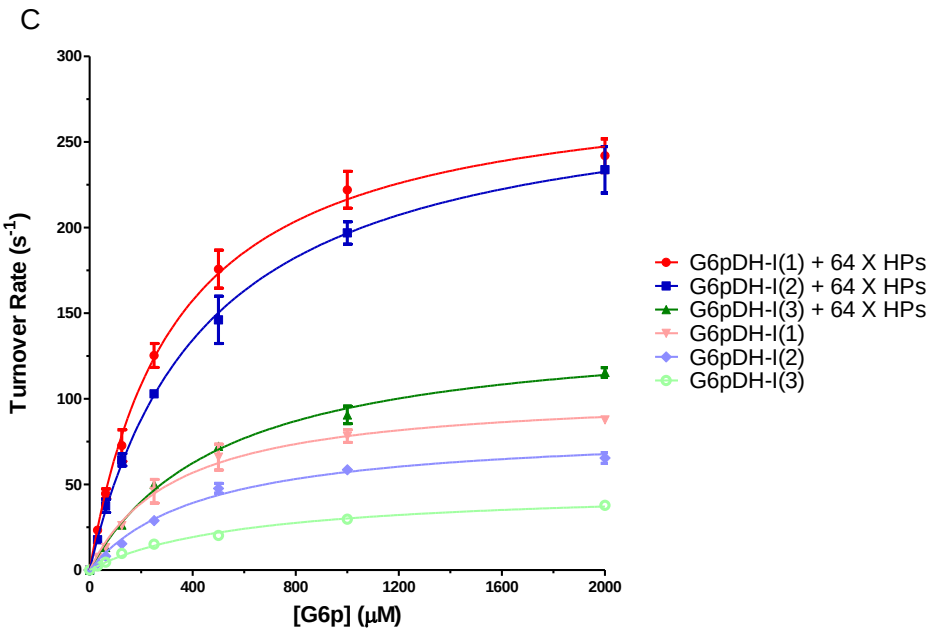

Figure 41: Substrate titration curves fitting for Km and kcat of individual enzyme-DNA nanoparticles and enzyme-initiator conjugates. (A) Titration of H_2O_2 for HRP samples. (B) Titration of NAD+ for G6PDH samples. (C) Titration of G6P for G6PDH samples. The conditions of the enzyme activity measurements can be found in the materials and methods section. Error bars represent the range of values for three replicates.

Enzyme	pI	Molecular Weight	Substrate	Enzyme-I		Enzyme-HCR	
				K_m (μM)	k_{cat}(s^{-1})	K_m (μM)	k_{cat}(s^{-1})
HRP-I(1)	8.8	44 kD	H_2O_2	19±2	84±2	19±1	137±2
HRP-I(2)	8.8	44 kD	H_2O_2	21±2	74±1	23±1	203±2
HRP-I(3)	8.8	44 kD	H_2O_2	19±1	77±1	24±1	225±3
G6PDH-I(1)	4.3	100 kD	G6P	335±44	105±5	333±30	289±9
			NAD^+	627±63	129±5	625±35	326±8
G6PDH-I(2)	4.3	100 kD	G6P	446±49	83±3	447±42	285±10
			NAD^+	673±78	133±7	673±68	378±16
G6PDH-I(3)	4.3	100 kD	G6P	602±52	48±2	519±42	144±5
			NAD^+	785±60	61±2	711±51	210±6

Table 2. Enzyme kinetic data (values of K_m and k_{cat}) for each individual DNA crowded enzyme nanoparticle in comparison with the values for enzyme-initiator conjugates. The pI values of the enzymes were obtained from brenda-enzymes.org. The error is represented as the standard error of three replicates.

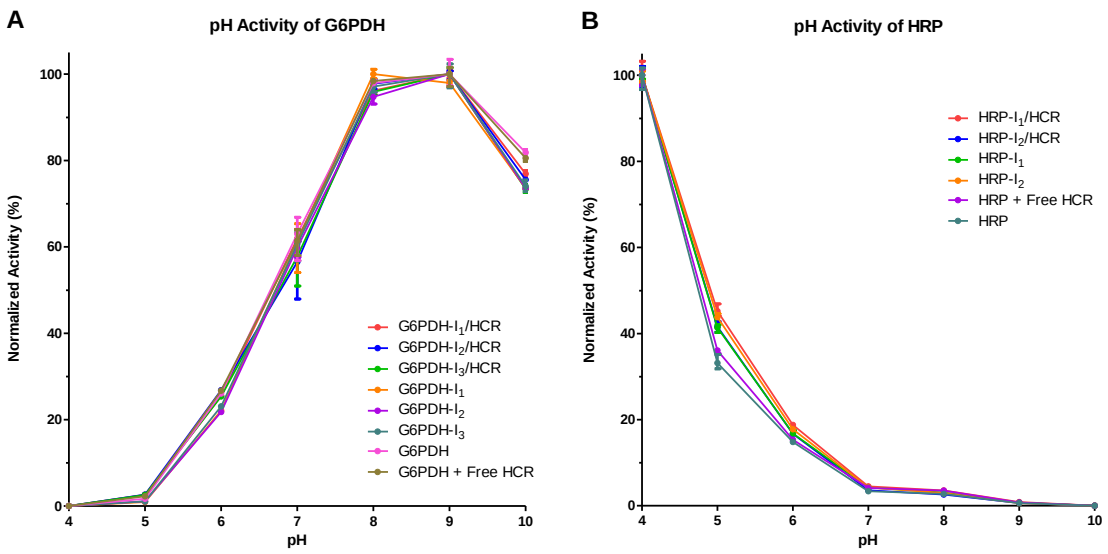

Figure 42. pH activities for (A) G6PDH-HCR nanoparticles and (B) HRP-HCR nanoparticles. Error bars represent the range of three replicates.

4.3.3. Stability Characterization of DNA-Crowded Enzyme Nanoparticles

In addition to enhancing the turnover numbers for catalysis, the DNA-crowded enzyme nanoparticles were also observed to increase the enzymes stability against various destabilizing conditions, such as long-term storage, freeze-thaw cycles, and thermal incubation. As shown in **Figure 43A**, the stability of enzyme solutions against long-term storage at room temperature (25 °C) was tested. All HRP-HCR complexes showed more stable activities as compared to HRP wildtype. For example, at the 10th week, HRP-HCR complexes retained ~ 50% of original activities, whereas HRP only retained ~20% of original activities. In **Figure 43B**, HRP-HCR complexes also showed increased stability against freeze-thaw cycles as compared to HRP wildtype, which is a major factor of protein denaturation in practical applications. It was also noticed that HRP-I_3/HCR (retain~ 90% activity at 10th cycle) was more stable than HRP-I_1/HCR

(retain~ 63% activity at 10th cycle) and HRP-I_2/HCR (retain~ 75% activity at 10th cycle), as well as HRP wildtype (retain~ 24% activity at 10th cycle). For a control experiment (**Figure 44)**, a Cy3-labelled enzyme was used to indicate the enzymes solution concentration during the testing period, by monitoring the solution fluorescence during the test period. The Cy3-labelled enzyme solution did not show a significant decrease in fluorescence during the test period, which suggested that there was a relatively stable concentration of solution enzyme. In **Figure 43C**, HRP-HCR complexes showed increased thermal stability of the enzyme from 45 – 65 °C.

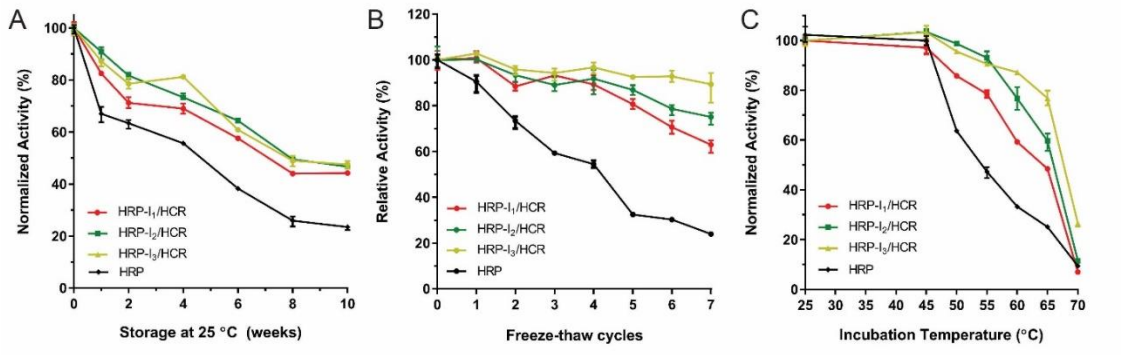

Figure 43. Evaluating the stability of DNA-crowded enzyme against (A) long-term storage under room temperature; (B) freeze-thaw cycles and (C) thermal incubation. Error bars represent the range of 3 replicates.

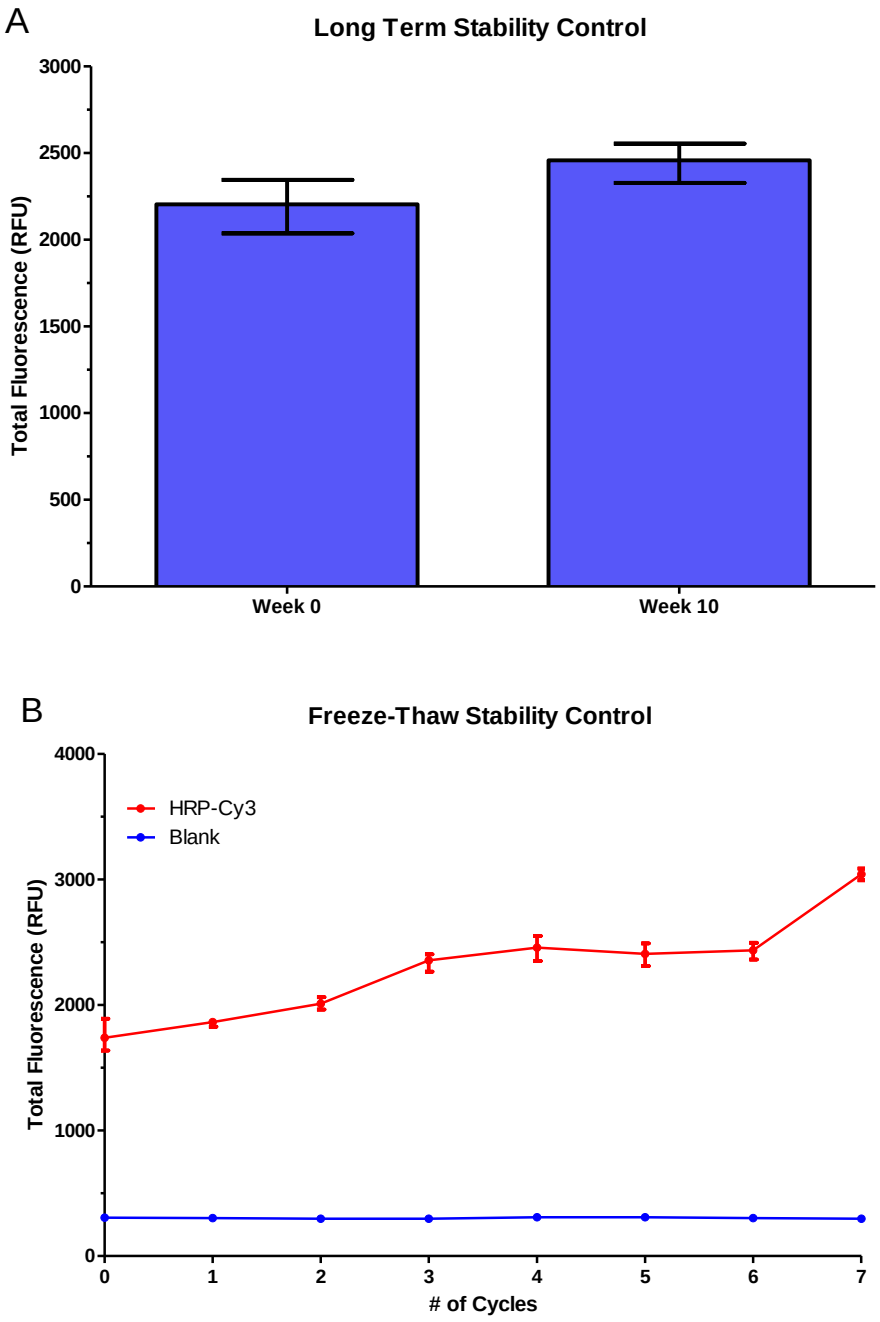

Figure 44. Control experiments using dye-labeled enzyme to ensure that the concentration of enzyme in solution does not decrease over the testing period. (A) Long term stability control. (B) Freeze-thaw stability control. Error bars represent the range of 9 replicates.

4.4. Conclusion

In summary, a robust and simple method for creating DNA-crowded enzyme nanoparticles with promoted enzyme activity and increased stability was developed. By conjugating an initiator strand to an enzyme, long DNA duplexes were able to be grown on the enzymes surface to increase local DNA crowding. The number and length of DNA duplexes were controlled by the copies of labelled DNA initiators and the addition of hairpins. The DNA-crowded enzyme nanoparticles exhibited increased turnover numbers of 2- to 3-fold higher than that of the free enzymes. Conversely, the K_m values remain similar between enzyme-HCR complexes and free enzymes, indicating an uninterrupted diffusion of small-molecule substrates and products through the surface-grown DNA duplexes. The enhanced activities of DNA-crowded enzyme nanoparticles were consistent with recently reported enzyme/DNA hybrid nanostructures, which might be attributed to the local DNA crowding with high density of negatively charged phosphate groups. This effect appears consistent with recent independent evidence that many conserved metabolic enzymes are stabilized by polyphosphate and associate non-specifically with nucleic acids through cryptic binding sites,[41, 91] thus taking advantage of the high polyanionic DNA and RNA contents of the cell. Unlike DNA origami nanocages with an application limit of low achievable concentrations, and the small production scale and high costs of complex oligonucleotides,[86a, 92] the assembly of DNA-crowded enzyme nanoparticles only involved three strands of one initiator and two hairpin substrates. The concentration and production of enzyme nanoparticles can be easily scaled up to high micro-molar concentrations for practical use. In the future, it may be feasible to crosslink multiple DNA-crowded enzyme nanoparticles into nanocrystals

and/or hydrogels which can stabilize enzymes against various denaturing conditions, as well as facilitating multi-enzyme catalysis. The DNA-crowded enzyme nanoparticles may also find utility in medical applications as therapeutic agents.

4.5. Acknowledgements

The following authors contributed to this work: John Collins, Ting Zhang, Sung Won Oh, and Jinglin Fu. This work is supported by an Army Research Office YIP award (W911NF-14-1-0434), the Cottrell College Science Award to J.F. and the start-up fund to J.F. from Rutgers University-Camden.

Concluding Remarks

Global environmental conditions play a critical role in the functional activity of enzymes. As demonstrated in chapters 2 and 3, the global environment surrounding Diaphorase played a critical role in allowing it to gain two new catalytic functions, that of a transhydrogenase and an oxidase. Changes in the reaction or storage conditions of the enzyme created substantial changes in its functional activities. These changes were simple given that the conditions used for these functional changes of the enzyme can be achieved in almost any laboratory. As demonstrated in chapter 4, the local crowding effect caused by DNA creates an optimal environment for the enzymes, boosting their activity as much as three-fold relative to that of the free enzyme, as well as significantly increasing their stability. This method for boosting the enzymes activities and stabilities was both simple and easy to prepare given it requires small amounts of DNA, and that the hybridization chain reaction can take place by simply mixing all strand species together in a one-pot procedure. The work done in this thesis demonstrates that industrial applications of enzymes can not only involve fine tuning the enzymes structure to affect its function, but also changing its surrounding environment to allow such changes to occur. This can allow for new and exciting ways to find more uses of enzymes in various industries, by tailoring their environment to meet the needs of the application. This opens up doors in industries by allowing for more wide-spread use of enzymes in industrial applications, as well as facilitating the use of a greener alternative to traditional chemical catalysts.

References

1. Vriezema, D. M.; Garcia, P. M. L.; Sancho Oltra, N.; Hatzakis, N. S.; Kuiper, S. M.; Nolte, R. J. M.; Rowan, A. E.; van Hest, J. C. M., Positional Assembly of Enzymes in Polymersome Nanoreactors for Cascade Reactions. *Angewandte Chemie International Edition* **2007,** *46* (39), 7378-7382.

2. Fu, J.; Liu, M.; Liu, Y.; Woodbury, N. W.; Yan, H., Interenzyme Substrate Diffusion for an Enzyme Cascade Organized on Spatially Addressable DNA Nanostructures. *Journal of the American Chemical Society* **2012,** *134* (12), 5516-5519.

3. Radzicka, A.; Wolfenden, R., A proficient enzyme. *Science* **1995,** *267* (5194), 90-93.

4. Wolfenden, R.; Snider, M. J., The Depth of Chemical Time and the Power of Enzymes as Catalysts. *Accounts of Chemical Research* **2001,** *34* (12), 938-945.

5. Voet, D. V., J. G.; Pratt, C. W., *Fundamentals of Biochemistry*. 2nd ed.; John Wiley & Sons: 2006.

6. https://www.memrise.com/mem/4808900/enzyme/.

7. Lehninger, A. L. N., D. L.; Cox, M. M., *Lehninger Principles of Biochemistry*. 6th ed.; W. H. Freeman and Company: New York, 2013.

8. (a) Scopes, R. K., Enzyme Activity and Assays. In *eLS*, John Wiley & Sons, Ltd: 2001; (b) Bisswanger, H., Enzyme assays. *Perspectives in Science* **2014,** *1* (1–6), 41-55.

9. http://themedicalbiochemistrypage.org/enzyme-kinetics.php#inhibitors.

10. (a) Cui, Y.; Cui, W.; Liu, Z.; Zhou, L.; Kobayashi, M.; Zhou, Z., Improvement of stability of nitrile hydratase via protein fragment swapping. *Biochemical and Biophysical Research Communications* **2014,** *450* (1), 401-408; (b) Chauhan, S.; Wu, S.; Blumerman, S.; Fallon, R. D.; Gavagan, J. E.; DiCosimo, R.; Payne, M. S., Purification, cloning, sequencing and over-expression in Escherichia coli of a regioselective aliphatic nitrilase from Acidovorax facilis 72W. *Applied Microbiology and Biotechnology* **2003,** *61* (2), 118-122.

11. (a) Savile, C. K.; Janey, J. M.; Mundorff, E. C.; Moore, J. C.; Tam, S.; Jarvis, W. R.; Colbeck, J. C.; Krebber, A.; Fleitz, F. J.; Brands, J.; Devine, P. N.; Huisman, G. W.; Hughes, G. J., Biocatalytic Asymmetric Synthesis of Chiral Amines from Ketones Applied to Sitagliptin Manufacture. *Science* **2010,** *329* (5989), 305-309; (b) Znabet, A.; Polak, M. M.; Janssen, E.; de Kanter, F. J. J.; Turner, N. J.; Orru, R. V. A.; Ruijter, E., A highly efficient synthesis of telaprevir by strategic use of biocatalysis and multicomponent reactions. *Chemical Communications* **2010,** *46* (42), 7918-7920.

12. Wang, Z.-X.; Shi, X.-X.; Chen, G.-R.; Ren, Z.-H.; Luo, L.; Yan, J., A new synthesis of α-arbutin via Lewis acid catalyzed selective glycosylation of tetra-O-benzyl-α-d-glucopyranosyl trichloroacetimidate with hydroquinone. *Carbohydrate Research* **2006,** *341* (11), 1945-1947.

13. (a) Haraguchi, K.; Yoshida, M.; Ohtsubo, K. i., Inulin fructotransferase (DFA III-producing) from Leifsonia sp. T88-4. *Carbohydrate Polymers* **2006,** *66* (1), 75-80; (b) Hang, H.; Miao, M.; Li, Y.; Jiang, B.; Mu, W.; Zhang, T., Difructosan anhydrides III preparation from sucrose by coupled enzyme reaction. *Carbohydrate polymers* **2013,** *92* (2), 1608-1611.

14. Yachmenev, V. G.; Bertoniere, N. R.; Blanchard, E. J., Intensification of the bio-processing of cotton textiles by combined enzyme/ultrasound treatment. *Journal of Chemical Technology & Biotechnology* **2002,** *77* (5), 559-567.

15. Maijala, P.; Kleen, M.; Westin, C.; Poppius-Levlin, K.; Herranen, K.; Lehto, J. H.; Reponen, P.; Mäentausta, O.; Mettälä, A.; Hatakka, A., Biomechanical pulping of softwood with enzymes and white-rot fungus Physisporinus rivulosus. *Enzyme and Microbial Technology* **2008,** *43* (2), 169-177.

16. Choi, J.-M.; Han, S.-S.; Kim, H.-S., Industrial applications of enzyme biocatalysis: Current status and future aspects. *Biotechnology Advances* **2015,** *33* (7), 1443-1454.

17. Kuznetsova, I. M.; Turoverov, K. K.; Uversky, V. N., What Macromolecular Crowding Can Do to a Protein. *International Journal of Molecular Sciences* **2014,** *15* (12), 23090-23140.

18. (a) Zimmerman, S. B.; Trach, S. O., Estimation of macromolecule concentrations and excluded volume effects for the cytoplasm of Escherichia coli. *Journal of Molecular Biology* **1991,** *222* (3), 599-620; (b) van den Berg, B.; Ellis, R. J.; Dobson, C. M., Effects of macromolecular crowding on protein folding and aggregation. *The EMBO Journal* **1999,** *18* (24), 6927-6933; (c) Rivas, G.; Ferrone, F.; Herzfeld, J., Life in a crowded world. *EMBO Reports* **2004,** *5* (1), 23-27.

19. Ellis, R. J.; Minton, A. P., Cell biology: Join the crowd. *Nature* **2003,** *425* (6953), 27-28.

20. Chaplin, M., Do we underestimate the importance of water in cell biology? *Nat Rev Mol Cell Biol* **2006,** *7* (11), 861-866.

21. (a) Minton, A. P., Influence of excluded volume upon macromolecular structure and associations in 'crowded" media. *Current Opinion in Biotechnology* **1997,** *8* (1), 65-69; (b) Minton, A. P., Implications of macromolecular crowding for protein assembly. *Current Opinion in Structural Biology* **2000,** *10* (1), 34-39.

22. Ralston, G. B., Effects of "crowding" in protein solutions. *Journal of Chemical Education* **1990,** *67* (10), 857.

23. Norris, M. G. S.; Malys, N., What is the true enzyme kinetics in the biological system? An investigation of macromolecular crowding effect upon enzyme kinetics of glucose-6-phosphate dehydrogenase. *Biochemical and Biophysical Research Communications* **2011,** *405* (3), 388-392.

24. Ma, B.; Xie, J.; Wei, L.; Li, W., Macromolecular crowding modulates the kinetics and morphology of amyloid self-assembly by β-lactoglobulin. *International journal of biological macromolecules* **2013,** *53*, 82-87.

25. Walde, P.; Ichikawa, S., Enzymes inside lipid vesicles: preparation, reactivity and applications. *Biomolecular Engineering* **2001,** *18* (4), 143-177.

26. (a) Price, A. D.; Zelikin, A. N.; Wang, Y.; Caruso, F., Triggered Enzymatic Degradation of DNA within Selectively Permeable Polymer Capsule Microreactors. *Angewandte Chemie International Edition* **2009,** *48* (2), 329-332; (b) Kreft, O.; Prevot, M.; Möhwald, H.; Sukhorukov, G. B., Shell-in-Shell Microcapsules: A Novel Tool for Integrated, Spatially Confined Enzymatic Reactions. *Angewandte Chemie International Edition* **2007,** *46* (29), 5605-5608; (c) Sakr, O. S.; Borchard, G., Encapsulation of Enzymes in Layer-by-Layer (LbL) Structures: Latest Advances and Applications. *Biomacromolecules* **2013,** *14* (7), 2117-2135; (d) Hosta-Rigau, L.; York-Duran, M. J.; Zhang, Y.; Goldie, K. N.; Städler, B., Confined Multiple Enzymatic (Cascade) Reactions within Poly(dopamine)-based Capsosomes. *ACS Applied Materials & Interfaces* **2014,** *6* (15), 12771-12779.

27. (a) Eggers, D. K.; Valentine, J. S., Crowding and hydration effects on protein conformation: a study with sol-gel encapsulated proteins11Edited by P. E. Wright. *Journal of Molecular Biology* **2001,** *314* (4), 911-922; (b) Eggers, D. K.; Valentine, J. S., Molecular confinement influences protein structure and enhances thermal protein stability. *Protein Science : A Publication of the Protein Society* **2001,** *10* (2), 250-261.

28. King, J. T.; Arthur, E. J.; Brooks, C. L.; Kubarych, K. J., Crowding Induced Collective Hydration of Biological Macromolecules over Extended Distances. *Journal of the American Chemical Society* **2014,** *136* (1), 188-194.

29. Seeman, N. C., Nucleic acid junctions and lattices. *Journal of Theoretical Biology* **1982,** *99* (2), 237-247.

30. (a) Linko, V.; Dietz, H., The enabled state of DNA nanotechnology. *Current Opinion in Biotechnology* **2013,** *24* (4), 555-561; (b) Jones, M. R.; Seeman, N. C.; Mirkin, C. A., Programmable materials and the nature of the DNA bond. *Science* **2015,** *347* (6224).

31. Rothemund, P. W. K., Folding DNA to create nanoscale shapes and patterns. *Nature* **2006,** *440* (7082), 297-302.

32. (a) Ke, Y.; Ong, L. L.; Shih, W. M.; Yin, P., Three-Dimensional Structures Self-Assembled from DNA Bricks. *Science* **2012,** *338* (6111), 1177-1183; (b) Ke, Y.; Ong, L. L.; Sun, W.; Song, J.; Dong, M.; Shih, W. M.; Yin, P., DNA brick crystals with prescribed depths. *Nat Chem* **2014,** *6* (11), 994-1002.

33. Li, H.; Park, S. H.; Reif, J. H.; LaBean, T. H.; Yan, H., DNA-Templated Self-Assembly of Protein and Nanoparticle Linear Arrays. *Journal of the American Chemical Society* **2004,** *126* (2), 418-419.

34. (a) Fu, J.; Yang, Y. R.; Dhakal, S.; Zhao, Z.; Liu, M.; Zhang, T.; Walter, N. G.; Yan, H., Assembly of multienzyme complexes on DNA nanostructures. *Nat. Protocols* **2016,** *11* (11), 2243-2273; (b) Yang, Y. R.; Liu, Y.; Yan, H., DNA Nanostructures as Programmable Biomolecular Scaffolds. *Bioconjugate Chemistry* **2015,** *26* (8), 1381-1395.

35. (a) Zhu, G.; Zheng, J.; Song, E.; Donovan, M.; Zhang, K.; Liu, C.; Tan, W., Self-assembled, aptamer-tethered DNA nanotrains for targeted transport of molecular drugs in cancer theranostics. *Proceedings of the National Academy of Sciences* **2013,** *110* (20), 7998-8003; (b) Wang, Z.-G.; Wilner, O. I.; Willner, I., Self-Assembly of Aptamer−Circular DNA Nanostructures for Controlled Biocatalysis. *Nano Letters* **2009,** *9* (12), 4098-4102.

36. Liu, M.; Fu, J.; Hejesen, C.; Yang, Y.; Woodbury, N. W.; Gothelf, K.; Liu, Y.; Yan, H., A DNA tweezer-actuated enzyme nanoreactor. *Nat Commun* **2013,** *4*.

37. Fu, J.; Yang, Y. R.; Johnson-Buck, A.; Liu, M.; Liu, Y.; Walter, N. G.; Woodbury, N. W.; Yan, H., Multi-enzyme complexes on DNA scaffolds capable of substrate channelling with an artificial swinging arm. *Nat Nano* **2014,** *9* (7), 531-536.

38. Rudiuk, S.; Venancio-Marques, A.; Baigl, D., Enhancement and Modulation of Enzymatic Activity through Higher-Order Structural Changes of Giant DNA–Protein Multibranch Conjugates. *Angewandte Chemie International Edition* **2012,** *51* (51), 12694-12698.

39. Timm, C.; Niemeyer, C. M., Assembly and Purification of Enzyme-Functionalized DNA Origami Structures. *Angewandte Chemie International Edition* **2015,** *54* (23), 6745-6750.

40. Zhao, Z.; Fu, J.; Dhakal, S.; Johnson-Buck, A.; Liu, M.; Zhang, T.; Woodbury, N. W.; Liu, Y.; Walter, N. G.; Yan, H., Nanocaged enzymes with enhanced catalytic activity and increased stability against protease digestion. *Nat Commun* **2016,** *7*.

41. Gray, Michael J.; Wholey, W.-Y.; Wagner, Nico O.; Cremers, Claudia M.; Mueller-Schickert, A.; Hock, Nathaniel T.; Krieger, Adam G.; Smith, Erica M.; Bender, Robert A.; Bardwell, James C. A.; Jakob, U., Polyphosphate Is a Primordial Chaperone. *Molecular Cell 53* (5), 689-699.

42. Sazanov, L. A., A giant molecular proton pump: structure and mechanism of respiratory complex I. *Nat Rev Mol Cell Biol* **2015,** *16* (6), 375-388.

43. (a) Kruger, N. J.; von Schaewen, A., The oxidative pentose phosphate pathway: structure and organisation. *Current Opinion in Plant Biology* **2003,** *6* (3), 236-246; (b) Jackson, J. B., A review of the binding-change mechanism for proton-translocating transhydrogenase. *Biochimica et Biophysica Acta (BBA) - Bioenergetics* **2012,** *1817* (10), 1839-1846.

44. Carlberg, I.; Mannervik, B., Purification by affinity chromatography of yeast glutathione reductase, the enzyme responsible for the NADPH-dependent reduction of the mixed disulfide of coenzyme A and glutathione. *Biochimica et Biophysica Acta (BBA) - Enzymology* **1977,** *484* (2), 268-274.

45. Sauer, U.; Canonaco, F.; Heri, S.; Perrenoud, A.; Fischer, E., The Soluble and Membrane-bound Transhydrogenases UdhA and PntAB Have Divergent Functions in NADPH Metabolism of Escherichia coli. *Journal of Biological Chemistry* **2004,** *279* (8), 6613-6619.

46. Pedersen, A.; Karlsson, G.; Rydström, J., Proton-translocating transhydrogenase: an update of unsolved and controversial issues. *Journal of Bioenergetics and Biomembranes* **2008,** *40* (5), 463-473.

47. (a) Cao, Z.; Song, P.; Xu, Q.; Su, R.; Zhu, G., Overexpression and biochemical characterization of soluble pyridine nucleotide transhydrogenase from Escherichia coli. *FEMS Microbiology Letters* **2011,** *320* (1), 9-14; (b) Egorov, M. V.; Tigerström, A.; Pestov, N. B.; Korneenko, T. V.; Kostina, M. B.; Shakhparonov, M. I.; Rydström, J., Purification of a recombinant membrane protein tagged with a calmodulin-binding domain: properties of chimeras of the Escherichia coli nicotinamide nucleotide transhydrogenase and the C-terminus of human plasma membrane Ca2+-ATPase. *Protein Expression and Purification* **2004,** *36* (1), 31-39; (c) Zhao, H.; Wang, P.; Huang, E.; Ge, Y.; Zhu, G., Physiologic roles of soluble pyridine nucleotide transhydrogenase inEscherichia coli as determined by homologous recombination. *Annals of microbiology* **2008,** *58* (2), 275-280.

48. Rice, L.; Phoenix, D. A.; Wainwright, M.; Waring, J. J., 19 Effect of increasing methylation on the ability of methylene blue to cause diaphorase-catalysed oxidation of NADH. *Biochemical Society Transactions* **1998,** *26* (4), S319-S319.

49. Catomeris, P.; Thibert, R. J., Study and optimization of the resazurin/diaphorase system. *Microchemical Journal* **1988,** *38* (3), 390-398.

50. Zhu, Z.; Kin Tam, T.; Sun, F.; You, C.; Percival Zhang, Y. H., A high-energy-density sugar biobattery based on a synthetic enzymatic pathway. *Nat Commun* **2014,** *5*.

51. Matsumoto, K. i.; Mukai, Y.; Ogata, D.; Shozui, F.; Nduko, J.; Taguchi, S.; Ooi, T., Characterization of thermostable FMN-dependent NADH azoreductase from the moderate thermophile Geobacillus stearothermophilus. *Applied Microbiology and Biotechnology* **2010,** *86* (5), 1431-1438.

52. Zhu, Z.; Zhang, Y. H. P., Use of nonimmobilized enzymes and mediators achieved high power densities in closed biobatteries. *Energy Science & Engineering* **2015**, n/a-n/a.

53. Hecht, H.; Erdmann, H.; Park, H.; Sprinzl, M.; Schmid, R., Crystal structure of NADH oxidase from Thermus thermophilus. *Nature Structural & Molecular Biology* **1995,** *2* (12), 1109-1114.

54. (a) Zhu, Z.; Sun, F.; Zhang, X.; Zhang, Y. H. P., Deep oxidation of glucose in enzymatic fuel cells through a synthetic enzymatic pathway containing a cascade of two thermostable dehydrogenases. *Biosensors and Bioelectronics* **2012,** *36* (1), 110-115; (b) Zhu, Z.; Wang, Y.; Minteer, S. D.; Percival Zhang, Y. H., Maltodextrin-powered enzymatic fuel cell through a non-natural enzymatic pathway. *Journal of Power Sources* **2011,** *196* (18), 7505-7509.

55. (a) Poinas, A.; Gaillard, J.; Vignais, P.; Doussiere, J., Exploration of the diaphorase activity of neutrophil NADPH oxidase. *European Journal of Biochemistry* **2002,** *269* (4), 1243-1252; (b) Reed, D. W.; Millstein, J.; Hartzell, P. L., H2O2-Forming NADH Oxidase with Diaphorase (Cytochrome) Activity from Archaeoglobus fulgidus. *Journal of Bacteriology* **2001,** *183* (24), 7007-7016; (c) Pessach, I.; Levy, R., The Nadph Oxidase Diaphorase Activity in Permeabilized Human Neutrophils and Granulocytic Like PLB-985 Cells. In *The Biology and Pathology of Innate Immunity Mechanisms*, Keisari, Y.; Ofek, I., Eds. Springer US: 2002; Vol. 479, pp 107-114.

56. You, C.; Zhang, X.-Z.; Zhang, Y.-H. P., Simple Cloning via Direct Transformation of PCR Product (DNA Multimer) to Escherichia coli and Bacillus subtilis. *Applied and Environmental Microbiology* **2012,** *78* (5), 1593-1595.

57. Wang, Y.; Huang, W.; Sathitsuksanoh, N.; Zhu, Z.; Zhang, Y. H. P., Biohydrogenation from Biomass Sugar Mediated by In Vitro Synthetic Enzymatic Pathways. *Chemistry & Biology* **2011,** *18* (3), 372-380.

58. (a) Lauterbach, L.; Idris, Z.; Vincent, K. A.; Lenz, O., Catalytic Properties of the Isolated Diaphorase Fragment of the NAD⁺-Reducing [NiFe]-Hydrogenase from <italic>Ralstonia eutropha</italic>. *PLoS ONE* **2011,** *6* (10), e25939; (b) Mukherjee, A.; Walker, J.; Weyant, K. B.; Schroeder, C. M., Characterization of Flavin-Based Fluorescent Proteins: An Emerging Class of Fluorescent Reporters. *PLoS ONE* **2013,** *8* (5), e64753.

59. (a) Butler, I. B.; Schoonen, M. A. A.; Rickard, D. T., Removal of dissolved oxygen from water: A comparison of four common techniques. *Talanta* **1994,** *41* (2), 211-215; (b) Zhao, C.; Bond, A. M.; Compton, R. G.; O'Mahony, A. M.; Rogers, E. I., Modification and Implications of Changes in Electrochemical Responses Encountered When Undertaking Deoxygenation in Ionic Liquids. *Analytical Chemistry* **2010,** *82* (9), 3856-3861.

60. (a) Florini, J. R., Assay of creatine kinase in microtiter plates using thio-NAD to allow monitoring at 405 nm. *Analytical biochemistry* **1989,** *182* (2), 399-404; (b) Anderson, W.; Fowler, W.; Pennington, R.; Fisher, R., Immunochemical characterization and purification of bovine heart mitochondrial pyridine dinucleotide transhydrogenase. *Journal of Biological Chemistry* **1981,** *256* (4), 1888-1895.

61. Bennett, B. D.; Kimball, E. H.; Gao, M.; Osterhout, R.; Van Dien, S. J.; Rabinowitz, J. D., Absolute metabolite concentrations and implied enzyme active site occupancy in Escherichia coli. *Nat Chem Biol* **2009,** *5* (8), 593-599.

62. Collins, J.; Zhang, T.; Huston, S.; Sun, F.; Zhang, Y. H. P.; Fu, J., A Hidden Transhydrogen Activity of a FMN-Bound Diaphorase under Anaerobic Conditions. *PLoS ONE* **2016,** *11* (5), e0154865.

63. (a) Neurath, H.; Greenstein, J. P.; Putnam, F. W.; Erickson, J. A., The Chemistry of Protein Denaturation. *Chemical Reviews* **1944,** *34* (2), 157-265; (b) Carpenter, J. F.; Manning, M. C.; Randolph, T. W., Long-Term Storage of Proteins. In *Current Protocols in Protein Science*, John Wiley & Sons, Inc.: 2001.

64. (a) Stirnemann, G.; Kang, S.-g.; Zhou, R.; Berne, B. J., How force unfolding differs from chemical denaturation. *Proceedings of the National Academy of Sciences* **2014,** *111* (9), 3413-3418; (b) Gray, Michael J.; Wholey, W.-Y.; Wagner, Nico O.; Cremers, Claudia M.; Mueller-Schickert, A.; Hock, Nathaniel T.; Krieger, Adam G.; Smith, Erica M.; Bender, Robert A.; Bardwell, James C. A.; Jakob, U., Polyphosphate Is a Primordial Chaperone. *Molecular Cell* **2014,** *53* (5), 689-699.

65. England, J. L.; Haran, G., Role of Solvation Effects in Protein Denaturation: From Thermodynamics to Single Molecules and Back. *Annual review of physical chemistry* **2011,** *62*, 257-277.

66. (a) Zhao, H.; Olubajo, O.; Song, Z.; Sims, A. L.; Person, T. E.; Lawal, R. A.; Holley, L. A., Effect of kosmotropicity of ionic liquids on the enzyme stability in aqueous solutions. *Bioorganic Chemistry* **2006,** *34* (1), 15-25; (b) Timasheff, S. N., Protein-solvent preferential interactions, protein hydration, and the modulation of biochemical reactions by solvent components. *Proceedings of the National Academy of Sciences* **2002,** *99* (15), 9721-9726; (c) Levy, Y.; Onuchic, J. N., Water and proteins: A love–hate relationship. *Proceedings of the National Academy of Sciences of the United States of America* **2004,** *101* (10), 3325-3326.

67. Ma, J.; Pazos, I. M.; Gai, F., Microscopic insights into the protein-stabilizing effect of trimethylamine N-oxide (TMAO). *Proceedings of the National Academy of Sciences* **2014,** *111* (23), 8476-8481.

68. (a) Miller, M. C.; Hanna, S. L.; DeFrates, K. G.; Fiebig, O. C.; Vaden, T. D., Kinetics and mass spectrometric measurements of myoglobin unfolding in aqueous ionic liquid solutions. *International Journal of Biological Macromolecules* **2016,** *85*, 200-207; (b) Takekiyo, T.; Yamazaki, K.; Yamaguchi, E.; Abe, H.; Yoshimura, Y., High ionic liquid concentration-induced structural change of protein in aqueous solution: A case study of lysozyme. *Journal of Physical Chemistry B* **2012,** *116* (36), 11092-11097; (c) Shu, Y.; Liu, M.; Chen, S.; Chen, X.; Wang, J., New insight into molecular interactions of imidazolium ionic liquids with bovine serum albumin. *Journal of Physical Chemistry B* **2011,** *115* (42), 12306-12314.

69. van Rantwijk, F.; Sheldon, R. A., Biocatalysis in ionic liquids. *Chemical Reviews* **2007,** *107* (6), 2757-2785.

70. (a) Laszlo, J. A.; Compton, D. L., Comparison of peroxidase activities of hemin, cytochrome c and microperoxidase-11 in molecular solvents and imidazolium-based ionic liquids. *Journal of Molecular Catalysis B: Enzymatic* **2002,** *18* (1–3), 109-120; (b) O'Reilly, N. J.; Magner, E., The effect of solvent on the catalytic properties of microperoxidase-11. *Physical Chemistry Chemical Physics* **2011,** *13* (12), 5304-5313.

71. Zhu, Z.; Sun, F.; Zhang, X.; Zhang, Y.-H. P., Deep oxidation of glucose in enzymatic fuel cells through a synthetic enzymatic pathway containing a cascade of two thermostable dehydrogenases. *Biosensors and Bioelectronics* **2012,** *36* (1), 110-115.

72. Zhu, A.; Romero, R.; Petty, H. R., An enzymatic fluorimetric assay for glucose-6-phosphate: application in an in vitro Warburg-like effect. *Analytical biochemistry* **2009,** *388* (1), 97-101.

73. (a) Sucharitakul, J.; Prongjit, M.; Haltrich, D.; Chaiyen, P., Detection of a C4a-Hydroperoxyflavin Intermediate in the Reaction of a Flavoprotein Oxidase. *Biochemistry* **2008,** *47* (33), 8485-8490; (b) Sucharitakul, J.; Wongnate, T.; Chaiyen, P., Hydrogen Peroxide Elimination from C4a-hydroperoxyflavin in a Flavoprotein Oxidase Occurs through a Single Proton Transfer from Flavin N5 to a Peroxide Leaving Group. *Journal of Biological Chemistry* **2011,** *286* (19), 16900-16909.

74. Golub, E.; Freeman, R.; Willner, I., A Hemin/G-Quadruplex Acts as an NADH Oxidase and NADH Peroxidase Mimicking DNAzyme. *Angewandte Chemie International Edition* **2011,** *50* (49), 11710-11714.

75. Mewies, M.; McIntire, W. S.; Scrutton, N. S., Covalent attachment of flavin adenine dinucleotide (FAD) and flavin mononucleotide (FMN) to enzymes: The current state of affairs. *Protein Science* **1998,** *7* (1), 7-20.

76. Greenfield, N. J., Using circular dichroism spectra to estimate protein secondary structure. *Nat. Protocols* **2007,** *1* (6), 2876-2890.

77. (a) Tollin, G., Magnetic circular dichroism and circular dichroism of riboflavine and its analogs. *Biochemistry* **1968,** *7* (5), 1720-1727; (b) D'Anna, J. A.; Tollin, G., Studies of flavine-protein interaction in flavoproteins using protein fluorescence and circular dichroism. *Biochemistry* **1972,** *11* (6), 1073-1080.

78. Hecht, H. J.; Kalisz, H. M.; Hendle, J.; Schmid, R. D.; Schomburg, D., Crystal Structure of Glucose Oxidase from Aspergillus niger Refined at 2·3 Å Reslution. *Journal of Molecular Biology* **1993,** *229* (1), 153-172.

79. Ferri, S.; Kojima, K.; Sode, K., Review of Glucose Oxidases and Glucose Dehydrogenases: A Bird's Eye View of Glucose Sensing Enzymes. *Journal of Diabetes Science and Technology* **2011,** *5* (5), 1068-1076.

80. Horaguchi, Y.; Saito, S.; Kojima, K.; Tsugawa, W.; Ferri, S.; Sode, K., Construction of Mutant Glucose Oxidases with Increased Dye-Mediated Dehydrogenase Activity. *International Journal of Molecular Sciences* **2012,** *13* (11), 14149.

81. Hartl, F. U.; Bracher, A.; Hayer-Hartl, M., Molecular chaperones in protein folding and proteostasis. *Nature* **2011,** *475* (7356), 324-332.

82. (a) Comellas-Aragones, M.; Engelkamp, H.; Claessen, V. I.; Sommerdijk, N. A. J. M.; Rowan, A. E.; Christianen, P. C. M.; Maan, J. C.; Verduin, B. J. M.; Cornelissen, J. J. L. M.; Nolte, R. J. M., A virus-based single-enzyme nanoreactor. *Nat Nano* **2007,** *2* (10), 635-639; (b) Liu, Y.; Du, J.; Yan, M.; Lau, M. Y.; Hu, J.; Han, H.; Yang, O. O.; Liang, S.; Wei, W.; Wang, H.; Li, J.; Zhu, X.; Shi, L.; Chen, W.; Ji, C.; Lu, Y., Biomimetic enzyme nanocomplexes and their use as antidotes and preventive measures for alcohol intoxication. *Nat Nano* **2013,** *8* (3), 187-192; (c) Sang, L.-C.; Coppens, M.-O., Effects of surface curvature and surface chemistry on the structure and activity of proteins adsorbed in nanopores. *Physical Chemistry Chemical Physics* **2011,** *13* (14), 6689-6698; (d) Vriezema, D. M.; Comellas Aragonès, M.; Elemans, J. A. A. W.; Cornelissen, J. J. L. M.; Rowan, A. E.; Nolte, R. J. M., Self-Assembled Nanoreactors. *Chemical Reviews* **2005,** *105* (4), 1445-1490.

83. Fu, J.; Liu, M.; Liu, Y.; Yan, H., Spatially-Interactive Biomolecular Networks Organized by Nucleic Acid Nanostructures. *Accounts of Chemical Research* **2012,** *45* (8), 1215-1226.

84. Ke, G.; Liu, M.; Jiang, S.; Qi, X.; Yang, Y. R.; Wootten, S.; Zhang, F.; Zhu, Z.; Liu, Y.; Yang, C. J.; Yan, H., Directional Regulation of Enzyme Pathways through the Control of Substrate Channeling on a DNA Origami Scaffold. *Angewandte Chemie International Edition* **2016,** *55* (26), 7483-7486.

85. Rudiuk, S.; Venancio-Marques, A.; Baigl, D., Enhancement and Modulation of Enzymatic Activity through Higher-Order Structural Changes of Giant DNA–Protein Multibranch Conjugates. *Angewandte Chemie* **2012,** *124* (51), 12866-12870.

86. (a) Zhao, Z.; Fu, J.; Dhakal, S.; Johnson-Buck, A.; Liu, M.; Zhang, T.; Woodbury, N. W.; Liu, Y.; Walter, N. G.; Yan, H., Nanocaged enzymes with enhanced catalytic activity and increased stability against protease digestion. *Nature Communications* **2016,** *7*, 10619; (b) Linko, V.; Eerikainen, M.; Kostiainen, M. A., A modular DNA origami-based enzyme cascade nanoreactor. *Chemical Communications* **2015,** *51* (25), 5351-5354.

87. (a) Gao, Y.; Roberts, C. C.; Zhu, J.; Lin, J.-L.; Chang, C.-e. A.; Wheeldon, I., Tuning Enzyme Kinetics through Designed Intermolecular Interactions Far from the Active Site. *ACS Catalysis* **2015,** *5* (4), 2149-2153; (b) Lin, J.-L.; Wheeldon, I., Kinetic Enhancements in DNA–Enzyme Nanostructures Mimic the Sabatier Principle. *ACS Catalysis* **2013,** *3* (4), 560-564.

88. Dirks, R. M.; Pierce, N. A., Triggered amplification by hybridization chain reaction. *Proceedings of the National Academy of Sciences of the United States of America* **2004,** *101* (43), 15275-15278.

89. Zhang, Y.; Tsitkov, S.; Hess, H., Proximity does not contribute to activity enhancement in the glucose oxidase–horseradish peroxidase cascade. *Nature Communications* **2016,** *7*, 13982.

90. (a) Zhao, H., Effect of ions and other compatible solutes on enzyme activity, and its implication for biocatalysis using ionic liquids. *Journal of Molecular Catalysis B: Enzymatic* **2005,** *37* (1), 16-25; (b) Moelbert, S.; Normand, B.; De Los Rios, P., Kosmotropes and chaotropes: modelling preferential exclusion, binding and aggregate stability. *Biophysical Chemistry* **2004,** *112* (1), 45-57; (c) Leberman, R.; Soper, A. K., Effect of high salt concentrations on water structure. *Nature* **1995,** *378* (6555), 364-366; (d) Jana, B.; Pal, S.; Maiti, P. K.; Lin, S.-T.; Hynes, J. T.; Bagchi, B., Entropy of Water in the Hydration Layer of Major and Minor Grooves of DNA. *The Journal of Physical Chemistry B* **2006,** *110* (39), 19611-19618; (e) Chuprina, V. P.; Heinemann, U.; Nurislamov, A. A.; Zielenkiewicz, P.; Dickerson, R. E.; Saenger, W., Molecular dynamics simulation of the hydration shell of a B-DNA decamer reveals two main types of minor-groove hydration depending on groove width. *Proceedings of the National Academy of Sciences of the United States of America* **1991,** *88* (2), 593-597.

91. Cieśla, J., Metabolic enzymes that bind RNA: yet another level of cellular regulatory network? *Acta Biochimica Polonica* **2006,** *53* (1), 11-32.

92. Jinglin Fu*, R. Y., Soma Dhakal, Zhao Zhao, Minghui Liu, Ting Zhang, Nils Walter and Hao Yan Assembly of Multi-Enzyme Complexes on DNA Nanostructures. *Nature Protocols* **2016,** *in press*.